ROLE OF SN IN THE PT/TIO2 CATALYST FOR THE SELECTIVE HYDROGENATION OF

FURFURAL TO FURFURYL ALCOHOL

By

MR. Nattaphat OVATNUPAT

A Thesis Submitted in Partial Fulfillment of the Requirements

for Master of Engineering (CHEMICAL ENGINEERING)

Department of CHEMICAL ENGINEERING

Graduate School, Silpakorn University

Academic Year 2021

ผลของดีบุกในตัวเร่งปฏิริยาแพลตตินัมบนตัวรองรับไททาเนียสำหรับปฏิกิริยาไฮโดรจิเนชัน แบบเลือกเกิดของเฟอร์ฟูรัลเป็นเฟอร์ฟูริลแอลกอฮอล

โดย
นายณัฏภัทร โอวาทนุพัฒน์

ROLE OF SN IN THE PT/TIO2 CATALYST FOR THE SELECTIVE

HYDROGENATION OF FURFURAL TO FURFURYL ALCOHOL

By

MR. Nattaphat OVATNUPAT

A Thesis Submitted in Partial Fulfillment of the Requirements

for Master of Engineering (CHEMICAL ENGINEERING)

Department of CHEMICAL ENGINEERING

Graduate School, Silpakorn University

Academic Year 2021

Title   ROLE OF SN IN THE PT/TIO2 CATALYST FOR THE SELECTIVE

                        HYDROGENATION OF FURFURAL TO FURFURYL ALCOHOL

By   MR. Nattaphat OVATNUPAT

Field of Study   (CHEMICAL ENGINEERING)

Advisor   Assistant Professor Choowong Chaisuk, D.Eng.

       Graduate School Silpakorn University in Partial Fulfillment of the Requirements for the Master of Engineering

--Dean of graduate school

(Associate Professor Jurairat Nunthanid, Ph.D.)

Approved by

--Chair person

   (Assistant Professor Tarawipa Puangpetch, Ph.D.)

--Advisor

   (Assistant Professor Choowong Chaisuk, D.Eng.)

--Committee

   (Nutchapon Chotigkrai, D.Eng.)

--External Examiner

   (Professor Joongjai Panpranot, Ph.D.)
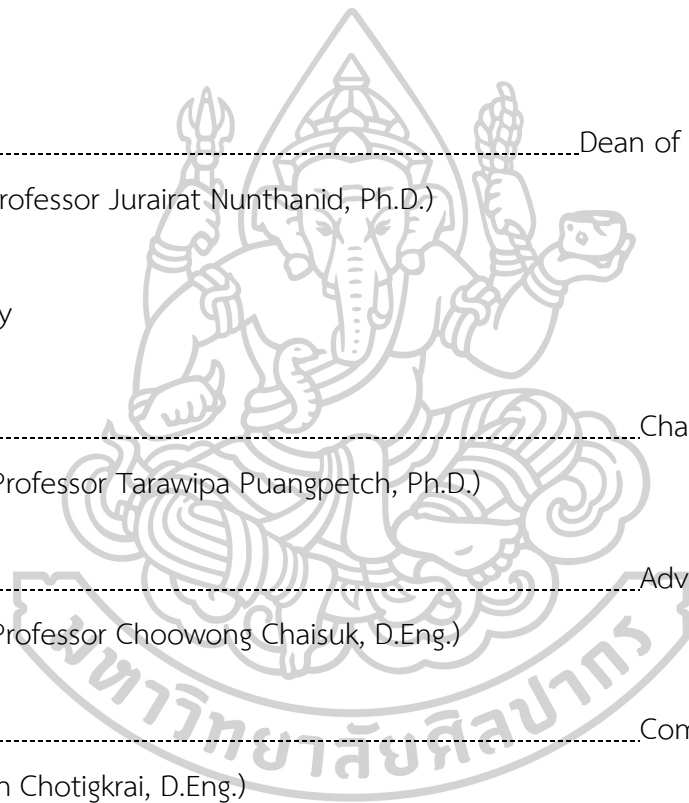
620920076 : Major (CHEMICAL ENGINEERING)

Keyword : Furfural hydrogenation, Furfuryl alcohol, Sn addition, Pt/TiO2, Pt catalyst, Flame spray pyrolysis

MR. NATTAPHAT OVATNUPAT : ROLE OF SN IN THE PT/TIO2 CATALYST FOR THE SELECTIVE HYDROGENATION OF FURFURAL TO FURFURYL ALCOHOL THESIS ADVISOR : ASSISTANT PROFESSOR CHOOWONG CHAISUK, D.Eng.

The effect of Sn loading in the Pt/TiO_2 catalyst on the selective hydrogenation of furfural to furfuryl alcohol was studied. The Sn with various loadings (0.1 – 1 wt%) was doped on TiO_2 support by wet impregnation method and subsequently 0.5 wt% Pt was re-impregnated on the Sn/TiO_2 material in the first part. In the second part, the catalyst with the suitable Sn loading in the first part was selected to study the change of the preparation methods, sequence impregnation, calcination temperature change and FSP (Flame spray pyrolysis). The catalyst was characterized by X-ray diffraction, N_2-physisorption, X-ray photoelectron spectroscopy, H_2-temperature programmed reduction and H_2 chemisorption. The activity, selectivity and stability of catalyst for the selective hydrogenation of furfural to furfuryl alcohol were evaluated. The presence of 0.5 wt% Sn loading exhibited the highest metal active sites confirmed by H_2 chemisorption. This was consistent with the highest activity and yield for the liquid-phase hydrogenation of furfural to furfuryl alcohol. The Pt catalyst supported on commercial P25 TiO_2 prepared by sequnce impregnation of Pt after Sn with calcination at low temperature showed the most performance in the furfural hydrogenation reaction.
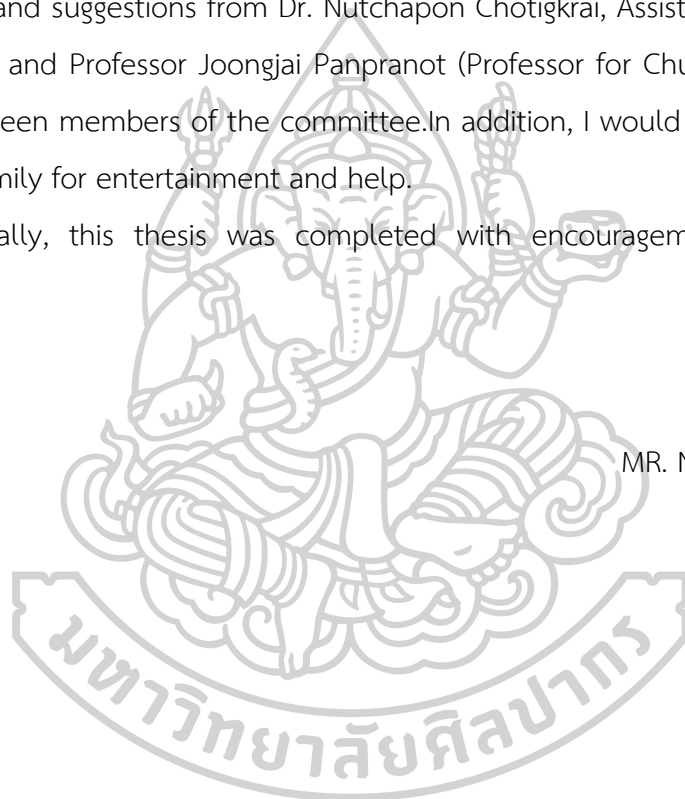
ACKNOWLEDGEMENTS

TABLE OF CONTENTS

LIST OF TABLES

LIST OF FIGURES

CHAPTER I

INTRODUCTION

1.1 Motivation

Furfural (FOL) derived from biomass, generally produced for industrial purposes. Obtained from dehydration of pentose. Which is the main ingredient in bio-oil [1]. The hydrogenation of furfural leading to products such as furfuryl alcohol (FA), tetrahydrofurfuryl alcohol (THFA), furan, 2-methylfuran (2-MF) and etc. Furfural lost up to 62% is estimated to be transformed into furfuryl alcohol (FA). This substance has received a lot of attention in the resin manufacturing process, synthesis of cross-linked polymers and solvent action [2]. In the industrial the hydrogenation of furfural to furfuryl alcohol, Chromite has traditionally been used as the catalyst [3]. However, chromium is toxic high to the environment. At present, most of the research is focused on the development of chromium-free catalysts.

Among the commonly used catalysts are Cu, Ni, Pd, Pt, Co, Rh, Ir and Ru. Pt-based catalyst shows good performance to hydrogenation furfural to furfuryl alcohol [4, 5]. However, it was also found that platinum, which is a group of 10 metals, has the ability to hydrogenation C=C bond easier than the C=O bond [6]. Which can increase the selection of hydrogenation C=O bond by addition of more electropositive metals. As a result, it can increase the energy to break the C=O bond [7]. The metal support TiO_2 there are widely used. Due to the ability to modify the properties of the catalyst phase of the support [8]. Pt/TiO_2 is substantiated to make H spillover, bring about to formation of the active furfuryl-oxy between the furfuraldehyde molecule and an O-vacancy site on the TiO_2 [9-11].

Previous studies have shown that the addition of Sn together with Ni-based catalyst, which is 10 metal groups. The results are in increased hydrogenation at the C=O bond, this is due to the addition this is due to the addition of electropositive metals in 10 metal group metals or the formation of the alloy to form an alloy, as a result of that affecting the high selectivity of furfuryl alcohol [12]. More research has been done that the bimetallic alloy is a more efficient catalyst in the field of activity and selectivity when compared to monometallic [13, 14]. Another also reduces the formation of organic fragments on the surface, allows for easy reuse [15, 16]. Therefore, make interest to study bimetallic between Pt-Sn base catalyst.

In this study, the bimetallic Pt-Sn load on TiO_2 support is investigated. The $Pt/Sn/TiO_2$ was prepared by wetness impregnation method in 2 steps. First step Sn was added on TiO_2 support after that Pt was added in same way. These catalysts are characterized by XRD, N_2-physisorption, TPR and H_2 chemisorption. The catalytic performances are evaluated by selective hydrogenation of furfural to furfuryl alcohol in a batch reactor and then analyzed by GC-FID.

1.2 Objective of Research

The aim of this research is to investigate the role of Sn in the $Pt/Sn/TiO_2$ catalyst on the selective hydrogenation of furfural to furfuryl alcohol in liquid phase.

1.3 Scope of Research

This research is divided into two parts.

The first part: Study effect of Sn loading in Pt based catalyst. The preparation of the $Pt/Sn/TiO_2$ catalyst were wet impregnation. **Table 1** shows the ratio of Pt and Sn in the catalyst. The catalyst was first impregnated by Sn and calcine after that impregnation by Pt.

Table 1 The percentage of Pt and Sn in the bimetallic.

	%wt in the Catalyst				
Pt	0.5	0.5	0.5	0.5	0.5
Sn	0	0.1	0.25	0.5	1

The second part: Study role of Sn by changing the preparation methods of the catalyst. The promising catalyst in the first part was selected to test in this part. Three methods were sequence impregnation, calcination temperature change and FSP (Flame spray pyrolysis).

1.4 Contribution of Research

Addition tin in Pt/TiO_2 catalyst can improve the activity and stability for the selective hydrogenation furfural to furfuryl alcohol in liquid phase
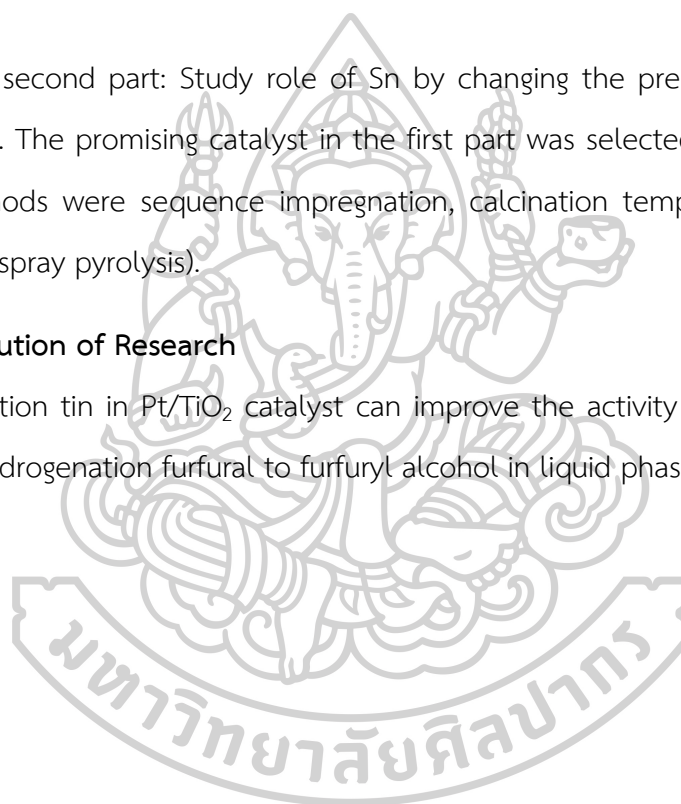
CHAPTER II

LITERATURE REVIEWS

2.1 Hydrogenation of furfural with heterogeneous catalyst

Furfural can be converted into a variety of solvents, polymers, fuels and other useful chemicals show in **Figure 1**. It is therefore of interest to develop. Hydrogenation of furfural up to 62% provides furfuryl alcohol for the production of furan resins used in thermoses composites.
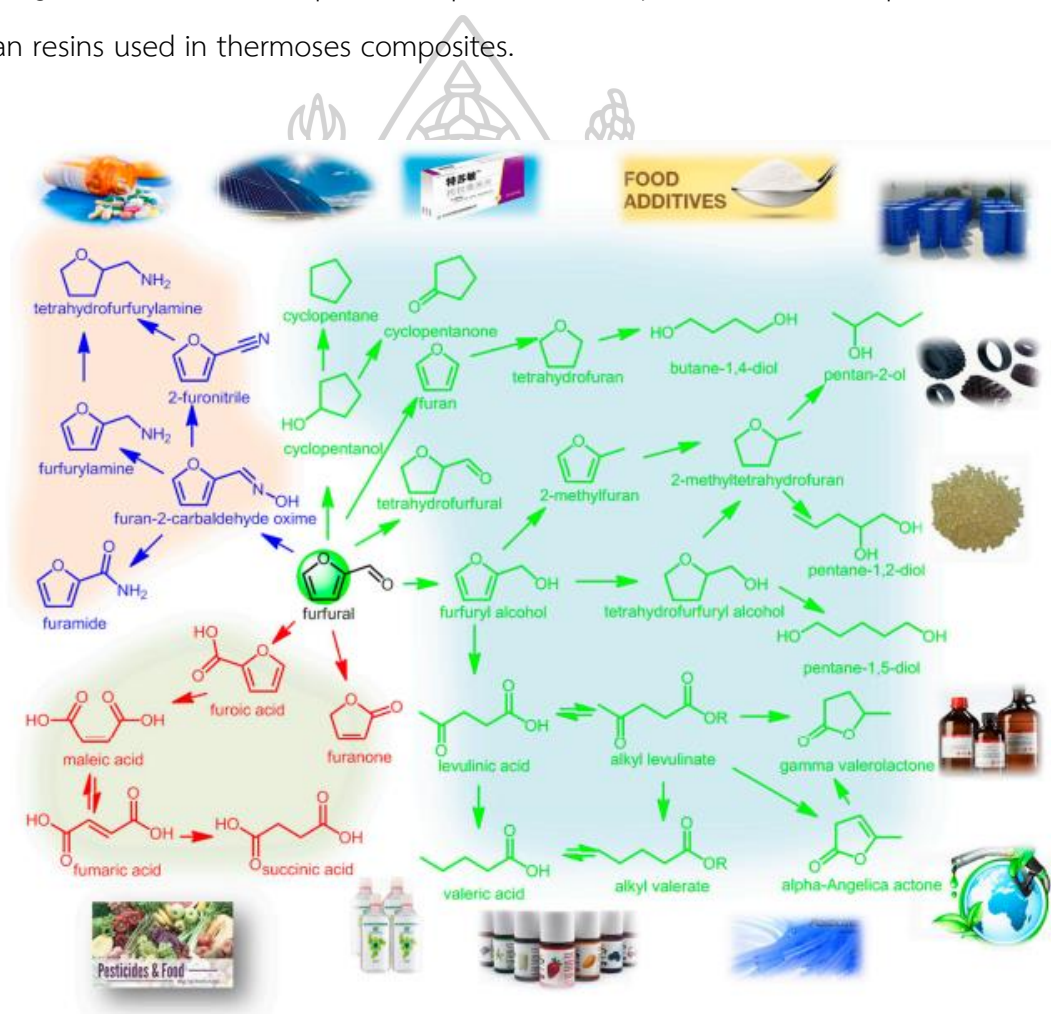
Figure 1 Downstream products of furfural, obtained by hydrogenation (in green), oxidation (in red), carnation, and other processes (in blue) [5].

Hydrogenation is a chemical reaction that occurs in unsaturated molecules in organic matter. It is a double bond in which a carbon atom with a hydrogen atom binds to a carbon atom until a single bond is formed around carbon atoms. This process is useful in pharmaceuticals and petrochemical industry. In industry, hydrogen gas is often used along with catalysts with metal catalysts. In this phase of substances are gas or liquid, but phase of catalyst is metal. Furfural hydrogenation is the addition of hydrogen gas to an Aldehyde functional group to obtain furfuryl alcohol with alcohol group. The main hydrogenation of furfural to furfuryl alcohol is

$$C_5H_4O_2 \text{ (furfural)} + H2 \longrightarrow C_5H_6O_2 \text{(furfuryl alcohol)}$$

However, furfural hydrogenation in liquid phase has been researched and developed extensively. Using supporting metals and amorphous alloys as catalysts. Most are copper chromite Cu, Ni, Mo, Co, Pt, Rh, Ru and Pd. Sometimes a second metal or promoter is added for improving the activity and the selectivity, by increasing the surface area or acting as Lewis's acid site to polarize the C=O bond. Furfural interacts with catalyst at the site via its carbonyl group oxygen show in **Figure 2**. Due to the adsorption, the C–O bond length of furfural is slightly increased desorption, while the C–C bond is decreased. The electron is transferred from the furfural oxygen atom to the catalyst. While nearby o atom gets more electron density. This shows that electrons are transferred to neighboring O atoms through active sites. Then H_2 molecule is then weakly bound to the adsorbed furfural. At the end, it is further converted to furfuryl alcohol via either the concerted or the stepwise pathway[17].
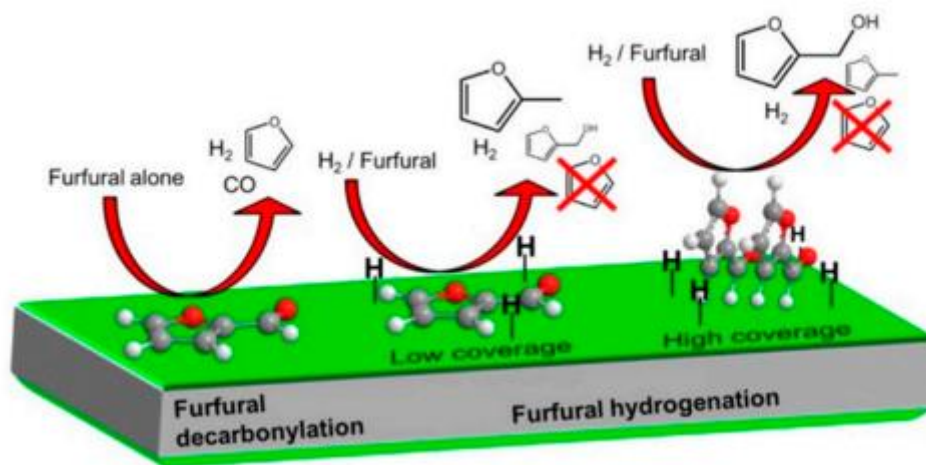
Figure 2 *Catalytic hydrogenation and hydrodeoxygenation of furfural over Pt(111) [18].*

2.2 Pt-based catalyst in furfural hydrogenation

Platinum is an element with atomic number 78 and symbol Pt. It is a silvery-gray, heavy-duty transition metal that can be stretched and plated. Platinum is extremely corrosion resistant. In nature found in nickel and copper ores, platinum does not react with oxygen (O) and therefore does not cause rust. Platinum can also be combined and mixed with other metals and also have strong durability Therefore, platinum is used to make a crucible with high heat resistance and platinum can also be used as a catalyst in chemistry reaction.

Platinum has been known as a furfural hydrogenation catalyst. It is widely used due to the unique electrical and chemical properties of the catalyst. Which has a positive effect on the reaction[19]. However, the commonly used platinum catalytic oxide in furfural hydrogenation usually also catalyzes unwanted side reactions and successive reactions, such as the hydrogenolysis of the C–O bond. Doping of supported platinum phase with electropositive transition metal (Sn, Fe, Ga). It's another interesting way to develop in select an unwanted partway [13, 16, 20, 21].

Taylor et al. [12] proposed Pt-Cu/Al$_2$O$_3$ in hydrogenation of liquid phase furfural at 50°C for 7 hr. The results of weight percent of Pt shown in **Figure 3**. Pt shown high yield more than Cu when mixed Pt and Cu at ultra-dilute 1:20 can improve conversion equivalent Pt catalyst.
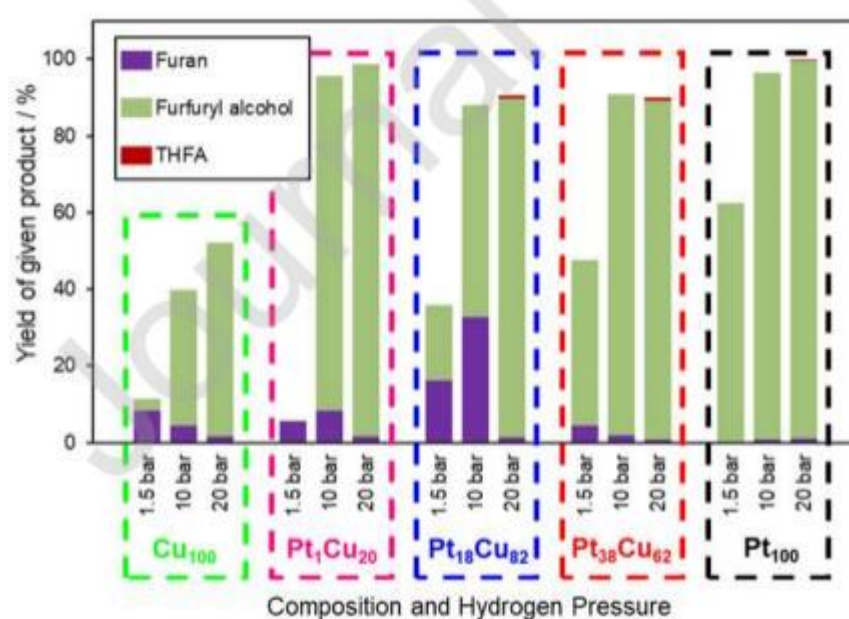
Figure 3 *Conversion and selectivity as an overall yield for each catalyst sample across three hydrogen pressures.*

Taylor et al. [20] proposed Pt nanoparticles were prepared adapting the method by variety of support catalysts. Catalyst evaluation at 50°C for 7 hr in ethanol solvent. The results in **Table 2** shown Pt can catalyze the reaction in liquid phase furfural hydrogenation well under mild conditions.

Table 2 *Furfural hydrogenation over Pt catalysts on support [20].*

Catalyst	Furfural conversion/%	Furfuryl alcohol selectivity/%	Furan selectivity/%	SP selectivity/%
Pt/γ-Al$_2$O$_3$	80	99	1	0
Pt/MgO	79	97	3	0
Pt/CeO$_2$	77	98	1	1
Pt/SiO$_2$	35	90	7	3
Pt/ZnO	7	60	40	0

2.3 Effect of Sn in catalyst

Tin is a chemical element with atomic number 50 and symbol is Sn. Tin is a bad metal. easily molten It is well oxidized in the air. But it is more resistant to corrosion than steel. found in many alloys Take advantage of metal coatings to prevent corrosion.

Rautio et al. [22] proposed The bimetallic catalyst was prepared by wet impregnation (Pt-Sn/TiO2). In hydrogenation of citral to geraniol(N) and nerol(G), which is hydrogenation at C=O as well as furfural hydrogenation to furfuryl alcohol shown in **Figure 4**. The hydrogenation of carbonyl bond in crotonaldehyde is reported to be more selective when Sn/Pt ratio is higher.
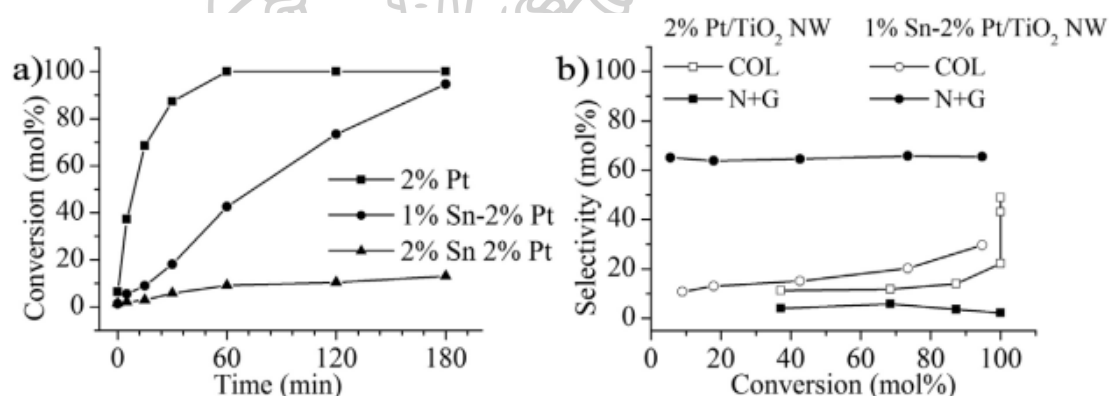
Figure 4 a) Conversion of citral in **2**-pentanol over **2** wt.% Pt/TiO$_2$ NW, **1** wt.% Sn-**2** wt.% Pt/TiO$_2$ NW and **2** wt.% Sn-**2** wt.% Pt/TiO$_2$ NW b) selectivity of **2** wt.% Pt/TiO$_2$ NW,**1** wt.% Sn-**2** wt.% Pt/TiO$_2$ NW [22].

Merlo et al. [15] proposed and investigated various Pt-Sn catalysts. Using ion exchange method to prepare Pt-Sn/SiO$_2$. The reaction using 0.25 g of catalyst and 2 ml of furfural in 50 ml of 2-propanol solvent at1.0 MPa H$_2$ pressure and 375K for 5 hr. The performance of Pt-Sn/SiO$_2$ shown in **Figure 5**. Adding Sn in the catalyst showed increased activity and stability in catalyst.
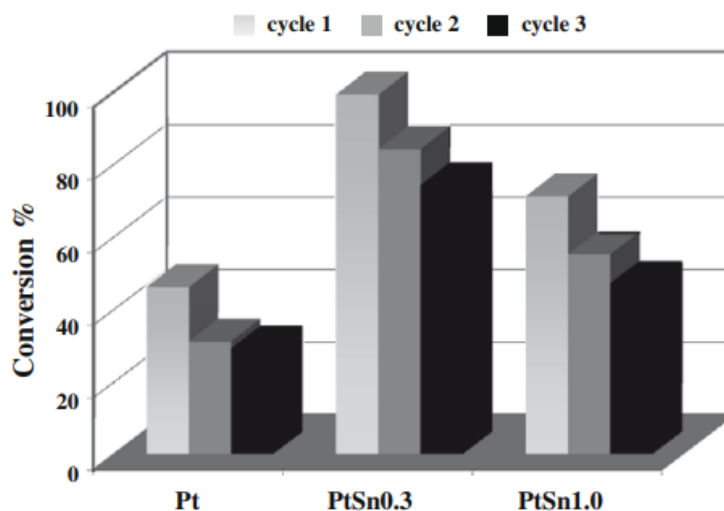
Figure 5 Activity of Pt, PtSn$_{0.3}$ and PtSn$_{1.0}$ for the furfural hydrogenation, in successive reactions [15].

O'Driscoll et al. [16] proposed effect of Sn about repeated hydrogenation cycles on furfural conversion in Pt catalyst co-impregnation. The result evaluation at 100 °C, H$_2$ pressure 20 bar,1 g of catalyst and 25 ml of furfural in 175 ml of toluene solvent shown in **Figure 6**. The Sn addition reduces the build-up of organic compounds on the catalyst surface, thereby increasing the efficiency of use over a longer period of time.
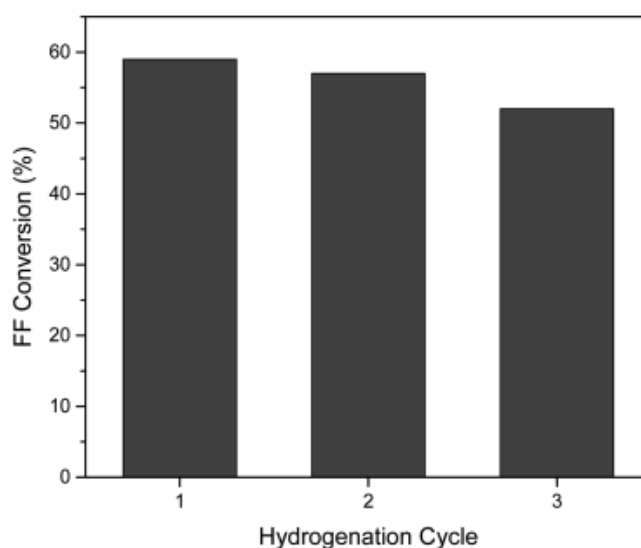
Figure 6 Effect of Pt-Sn/SiO$_2$ repeated cycles on furfural conversion [16].

Jerdev et al. [23] propose that this result is due to Sn loosening to form the SnO$_x$ adlayer during oxidation. This was followed by reduction of the Sn oxidized to the inactive metal Sn adlayer during low-temperature catalytic reactions. The catalytic ability of the pre-oxidized alloy can be restored for alloys prepared by H$_2$ reduce at temperatures in excess of 600 K.

Wettstein et al. [24]The addition of Sn leads to the formation of Ru–Sn bimetallic alloys such as Ru$_2$Sn$_3$ and Ru$_3$Sn$_7$. These alloys have lower rotational frequencies for hydrogenation reactions compared to the monometallic Ru phase. The amount of Sn produces an additional phase β-Sn, which is inactive in hydrogenation, instantaneous incineration and leaching under reaction conditions. Among the catalysts studied, RuSn$_4$/C proved stable even when LA produced.

Liu, M., et al.[25] propose SnO$_2$ partially covered the Pt nanoparticle surface when compared to the control Pt nano catalyst. The Pt-SnO$_2$ nano catalyst showed catalyst activity and selectivity for hydrogenation. The nitro aromatics displaced on Pt-SnO$_2$ were not reduced even though the Pt surface was partially covered by the SnO species and the product molecules could be released from the catalyst surface. easier, which results in a faster response rate. It can be concluded that the increased catalytic efficiency of Pt-SnO$_2$/Al2O$_3$ Derived from the interaction of Pt-SnO$_2$ within different nanostructures.

Stagg, S.M., et al. [26] propose although an increase in Sn reduces carbon deposition.But we believe that the negative effect of Sn is to intercept Pt interactions with support. To mitigate the negative effects of Sn, we used a preparatory method that allowed for the controlled addition of a small amount of Sn to reduce the carbon well position without compromising the role of support. Methods for reducing

surface deposition have a specific effect. The position of Sn on the pre-reduced Pt particle. This eliminates the possibility of excess Sn interacting with support. This technique also allows the placement of Sn is controlled by changing the size of the ligand.

2.4 Study effect of TiO$_2$ support catalyst

Titanium dioxide (TiO$_2$) has received attention in hydrogenation reaction. Found that a supporting structure for Titania. It has a great effect on the catalytic efficiency of the catalyst in the hydrogenation reaction due to the difference in titania. The structure will result in different physicochemical properties and catalyst properties [8]. Evonik Aeroxide TiO$_2$ P25 (formerly known as Degussa P25 , and hereafter referred to as P25), synthesized via flame pyrolysis of TiCl$_4$, is widely used because the presence of the Anatase Phase greatly increases the hydrogenation efficiency [11].

Table 3 Physic properties of TiO2 P25 [27].

Molecular formular	TiO$_2$
Molecular weight	79.87
From	Solid
Density (g/cm^3)	4.26
Anatase Phase (%)	76.3±1.5
Rutile Phase (%)	10.6±0.3
Amorphous (%)	13.5±1.5

Kijenski et al. [28] proposed effect of Pt on oxide support prepared by precipitation. Result of hydrogenation of furfural at 423 K shown in **Figure 7**. Titania demonstad best catalytic efficiency in all oxide support that have been studied in research.
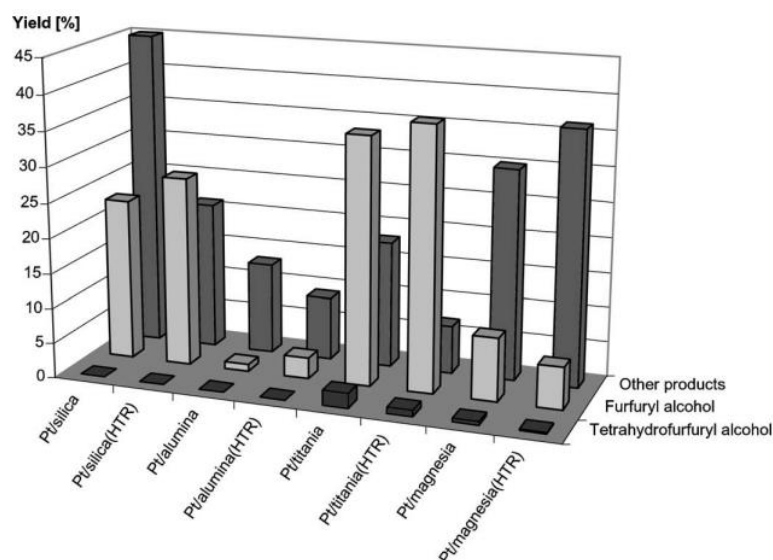
Figure 7 The yields of furfural hydrogenation products in the presence of platinum/metal oxide systems.

Li, F., et al. [29] The addition of TiO2 results in better dispersion of the active components. Cu crystal particle growth was slower, and Cu to Cu was reduced faster. The enhancement of Cu electronegativity in Cu/TiO2-SiO2 catalyst catalyzed the hydrogenation of C=O. This catalyst reduction temperature the sintering temperature and Cu loading also significantly affect the catalyst efficiency of the catalyst.

2.5 Effect of difference catalyst properties.

O'Driscoll, Á., et al.[16]the support framework may be affected such as the collapse of some pore walls to form very large pores which would reduce the interaction between the catalyst and the reactant. Additionally, at a higher

temperature the metal particles may agglomerate. which may result in a reaction shown in **Figure 8**.
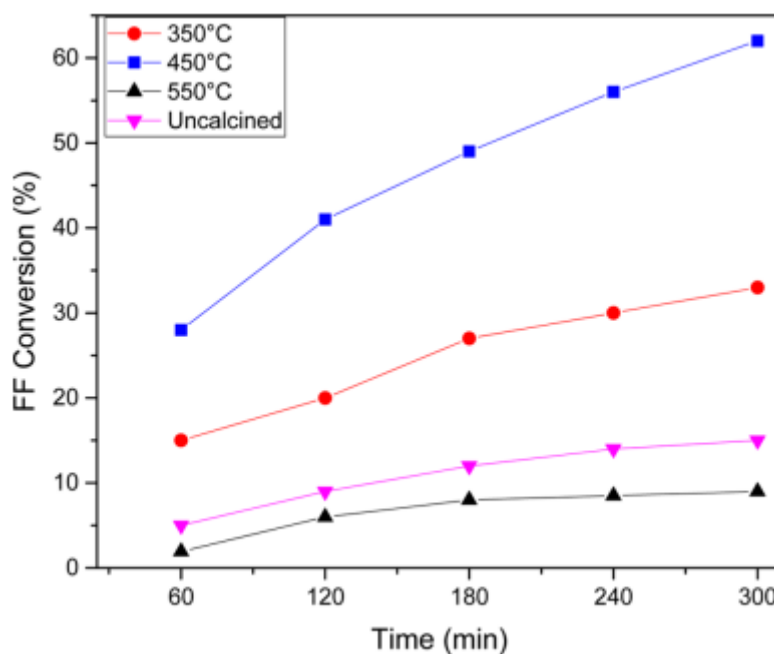
Figure 8 Influence of calcination temperature on 0.7%Pt–0.3%Sn/SiO$_2$.

Pisduangdaw, S., et al.[30] supported Pt–Sn/Al$_2$O$_3$ catalysts synthesized by one-step FSP method exhibited higher catalytic activity and better stability in the dehydrogenation of propane with high propylene selectivity compared to the ones prepared by conventional impregnation shown in **Figure 9**.
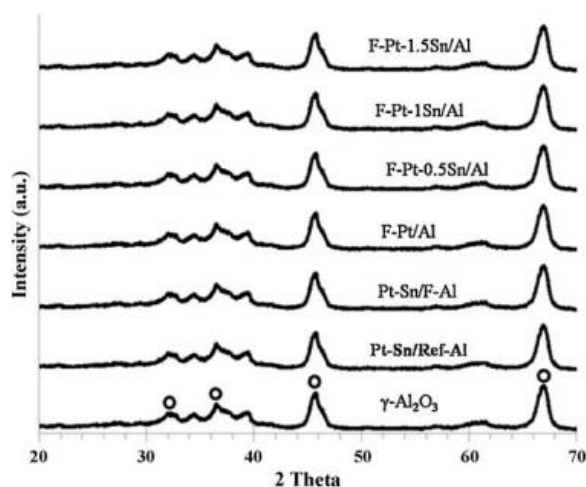
Figure 9 XRD patterns of the flame-made Pt–Sn/Al$_2$O$_3$ catalysts (as synthesized).

Paulauskas, et al.[31] propose the synthesis of TiO$_2$ with Al and Sn respectively significantly altered the phase ratio shown in **Figure 10**, with the rutile phase being the dominant phase in each sample, as anticipated. The TiO$_2$/Sn sample showed a higher proportion of rutile phase to anatase, despite having a lower at% of the composite metal compared to the TiO$_2$/Al sample.
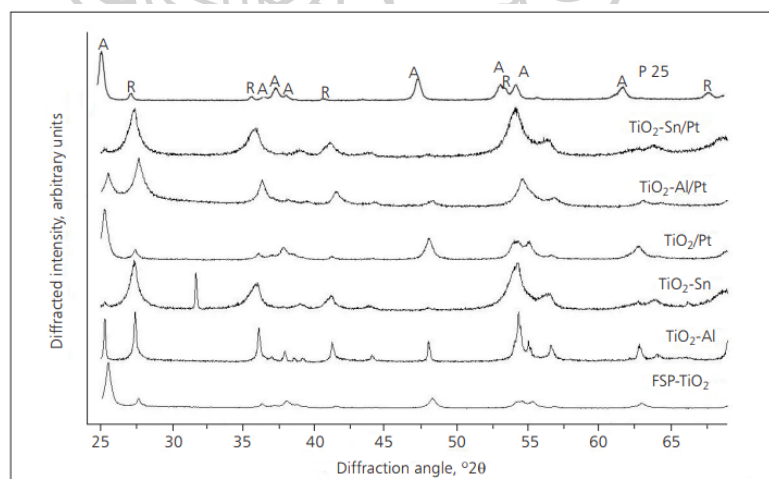
Figure 10 XRD diffraction patterns for the six TiO2 based FSP synthesized materials and the commercially available P25 sample for reference. Peaks representative of the anatase (A) and rutile (R) phases are labelled accordingly.

Tang, X., et al. [32] said for samples burned below 773 K, two reduction peaks at approximately 640 and 700 K were clearly observed shown in **Figure 11** . The low-temperature reduction peak may be due to the reduction of MnO_2 to Mn_3O_4, and the high-temperature reduction peak was defined as the reduction of Mn3O4 to MnO in conjunction with the reduction of the CeO_2 surface. gradually combined with a single reduction peak and shifted to higher temperatures with an increase in the sintering temperature to 973 K. This results in a reduction of pure MnO_2. This may indicate that the MnO_x phase was separated from the MnO_x–CeO_2 solid solution at sintering temperatures above 773 K.
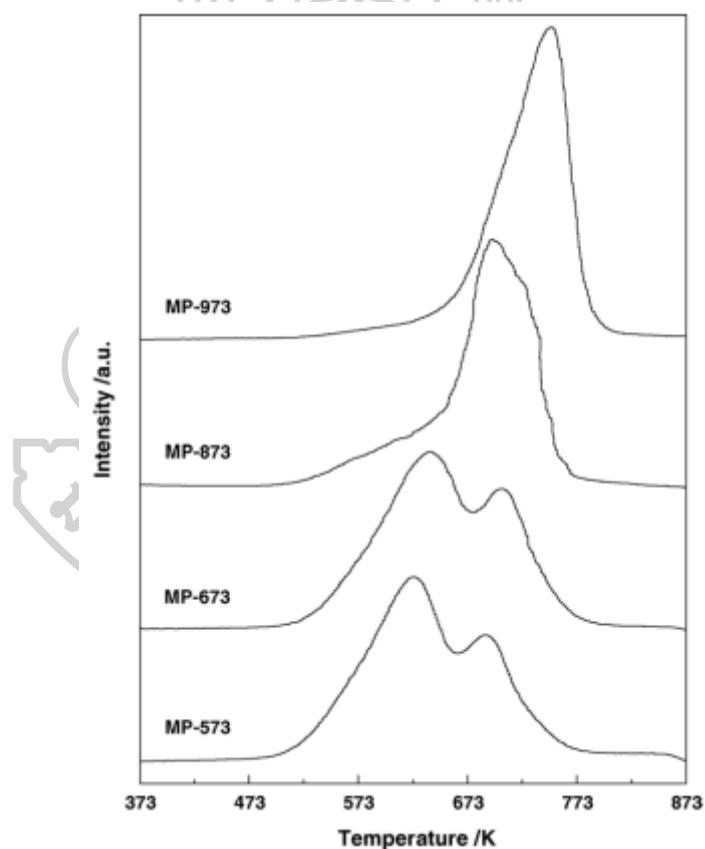
Figure   11 H_2-TPR profiles of the MnO_x–CeO_2 catalysts.

2.5 Wet impregnation method.

Wet impregnation method is a common technique for the synthesis of heterogeneous catalysts. Typically, the active metal precursor is dissolved in an aqueous or organic solution. Then, a solution containing the metal is added to the pore volume catalyst. The porosity is equal to the volume of the added solution. The capillary action draws the solution into the pores. The added solution beyond the supporting pore volume causes the solution transport to change from the capillary process to the diffusion process. This is much slower. The catalyst can then be dried and burned to expel the volatile components within the solution. by placing the metal on the surface of the catalyst.

Gurbani, A., et al.[33] Propose the conventional WI-prepared CuO–CeO$_2$ catalyst showed excellent activity and selectivity. as well as high surface area and good interaction with CO due to the extremely small particle size. It seems that the necessary reaction between the metal and the support is effective. Catalyst efficiency is achieved by simple preparation methods such as wet plating to achieve a large Cu–Ce interface.

2.6 Flame spray pyrolysis method.

Flame spray pyrolysis is a synthesis of combustion, which makes the liquid metal precursors in powder form with a high surface area and a small nanometer scale. The solution containing the metal and solvent components is dispersed into a flame. The combustion causes a small cluster and high temperature combustion. Due to the oxygen gas content and the high temperature of the flame. The nanoparticles made of flame spray pyrolysis are oxidized and crystalline. Powder is collected by a filter system that is above the flame. After the process is finished,

Nano-particles are ready to use immediately Nano-particle production process is shown in **Figure 12**.
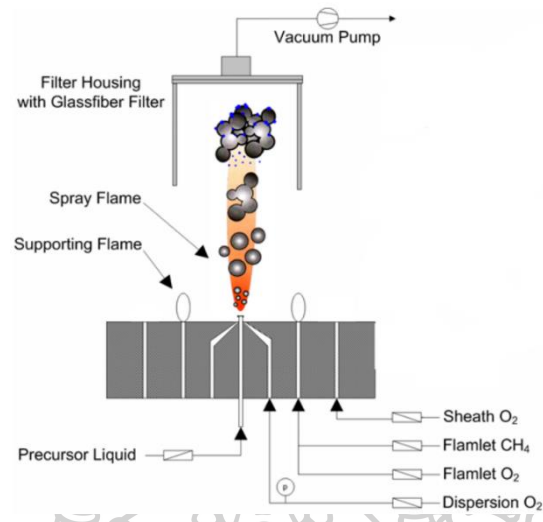
Figure 12 Nanoparticle production process.

Høj et al. [34] Studied Flame spray synthesis of CoMo/Al2O₃ hydrotreating catalysts. Catalysts were prepared by one-step flame spray pyrolysis (FSP). The catalysts showed high activity and high selectivity towards direct desulfurization, indicating that the desired promoted Co–Mo–S phase was formed upon sulfidation of the oxide flame synthesis product, despite formation of some $CoAl_2O_4$ during the flame synthesis.

Simmance et al. [35] Studied Evaluation of perovskite catalysts prepared by flame spray pyrolysis for three-way catalyst activity under simulated gasoline exhaust feeds. Catalysts were synthesised by liquid feed flame spray pyrolysis. High surface area perovskites can be synthesized using liquid feed flame spray pyrolysis. The FSP technique has been shown to be flexible in preparing a wide range of perovskite compositions and stoichiometries with good phase purity.

Panpranot et al. [36] reported that different Pd/SiO2 catalyst preparations between Flame Spray pyrolysis and Impregnation, which are shown in **Table 4**. The flame-induced catalyst increases the BET surface area when palladium is added from 0 to 5 percent by weight and change static for 10 percent by weight, but the impregnating catalyst formed, the BET surface area decreased with increasing. Palladium load from 0 to 10 percent weight.

Table 4 *Physicochemical properties of flame spray pyrolysis and Impregnation-made Pd/SiO$_2$ catalysts.*

catalyst	BET surface area (m^2/g)	Particle Size (nm)		pore volume (cm^3/g)	average pore size (Å)
		SiO$_2$	Pd phase		
				Flame-Made Catalysts	
SiO$_2$	196	14.0	n/a[a]	0.48	90.0
0.5% Pd/SiO$_2$	246	11.1	n.d.[b]	0.43	67.3
1% Pd/SiO$_2$	251	10.9	n.d.[b]	0.46	73.7
2% Pd/SiO$_2$	260	10.9	n.d.[b]	0.49	77.6
5% Pd/SiO$_2$	306	8.9	n.d.[b]	0.59	76.1
10% Pd/SiO$_2$	299	9.1	2.8	0.69	90.9
				Impregnation-Made Catalysts	
0.5% Pd/SiO$_2$	174	15.7	n.d.[b]	0.91	204.4
1% Pd/SiO$_2$	171	15.9	n.d.[b]	0.91	193.5
2% Pd/SiO$_2$	133	20.5	n.d.[b]	0.60	249.1
5% Pd/SiO$_2$	109	25.0	12.4	0.47	143.5
10% Pd/SiO$_2$	128	21.3	5.2	0.50	168.2

[a] Not available. [b] Not determined.

CHAPTER III

RESEARCH METHODOLOGY

3.1 Materials

The precursor and solvent for synthesis catalyst show in **Table 5.**

Table 5 the details of chemicals used for catalyst preparation.

Symbol		Chemicals	Formula
Precursor	**Platinum**	Platinum (II) acetylacetonate	$C_{10}H_{14}O_4Pt$
	Tin	Tin (II) chloride dihydrate	$Cl_2Sn \cdot 2H_2O$
	Titania	Titanium Dioxide P25	TiO_2
	Titania	Titanium (IV) butoxide	$Ti(OCH_2CH_2CH_2CH_3)_4$
Solvent		**Xylene**	$C_6H_4(CH_3)_2$

3.2 Catalyst preparation

3.2.1 Wet impregnation method

The aqueous precursor Tin (II) chloride dihydrate 15ml dropped on the Titanium Dioxide P25 (TiO_2) support. Stirrer solution was held at 70ºC for 6h. Oven at 110ºC for 12h. Crush the catalyst to powder and calcine in 50 ml/min of air flow at 450ºC for 3h. Final aqueous precursor Platinum (II) acetylacetonate 15ml dropped on the support. Stirrer solution was held at 70ºC for 6h. Oven at 110ºC for 12h. Crush the catalyst to powder and calcine in 50 ml/min of air flow at 450ºC for 3h.

3.2.2 Flame spray pyrolysis

flame spray pyrolysis reactor was employed. The Xylene solvent has diluted the titanium and tin precursors to a concentration of 0.5 M. The liquid precursor was supplied at a rate of 5 ml/min using a syringe pump. At a rate of 5 L/min, oxygen was distributed. At 1.5 bar, the pressure drop at the nozzle was constant. With the help of a vacuum pump, the catalyst powder was collected on a filter. Pt was loaded using the wet impregnation technique. Finally, the powder was calcined at 400 °C for 4 hours

3.3 Catalyst characterization

3.3.1 X-ray diffraction (XRD)

The XRD measurement was used to determine the bulk crystalline phases of catalysts sample in the range 2θ from 20° to 80° with Pt and Sn Kα. The crystallite sizes were determined from XRD data using the Scherer equation.

3.3.2 Nitrogen physisorption

N_2 physisorption was used to determine the BET surface area of catalyst, the average pore size diameter. Use helium flow rate 50 ml/min at 150°C for 3h for characterize catalyst.

3.3.3 Temperature programed reduction (TPR)

The hydrogen temperature programmed reduction (H_2-TPR) was used to determined bulk reduction behavior and the reducibility of catalyst The behavior of catalyst was measured by a Micrometritrics AutoChem 2910 instrument.

Catalyst samples 0.1 g of was added in a quartz tubular reactor. Using nitrogen atmosphere at flow rate of 30 ml/min, the catalyst sample was heat up to 150 °C, heating rate of 10 °C/min and held at 150 °C for 1 h The reducing

step is processed under 10% H_2 in N_2 was switched on the catalyst at 30ml/min from room temperature to 800 °C at the ramp heating rate of 10 °C/min and held at 800 °C for 1 h.

3.3.4 Hydrogen chemisorption

Hydrogen chemisorption was used to determine the Active sites of catalyst The behavior of catalyst was measured by a Micrometritrics AutoChem 2910 instrument

Catalyst samples 0.1 g of was added in a quartz tubular reactor or glass tubular reactor. Flowing nitrogen over catalyst while ramping the temperature at 500 °C. The catalyst was reduced in hydrogen heated to 500 °C and heals 1h. After that cool down to 100 °C. The metal active sites were measured at 100 °C. Start analysis the pure hydrogen gas (50µl) was injected in to the port to adsorb on the metal of the catalyst. Repeated injected hydrogen until catalyst saturation. Take the data was calculation using the method described by Reuel and Bartholome.

3.3.5 X-ray photoelectron spectra (XPS)

X-ray photoelectron spectra of catalyst samples were performed by using the Kratos Amicus x-ray photoelectron spectroscopy, the blinding energy was referenced to C 1s line (at 284.6 eV). The binding energy (BE) of Pt 4p are determined (at 74.5).

3.4 Catalyst evaluation

3.4.1 Activity evaluation

Catalyst was reduced by H_2 at 500°C for 1 hr. The reaction using 0.05 g of catalyst and 0.1 ml of furfural in 10 ml of 2-propanol solvent at 20 bar H_2 pressure and 80 °C 2 hr in stainless steel reactor. The liquid product was analyzed by GC-FID detector.

3.4.2 Stability evaluation

Catalyst was tested in activity evaluation will be centrifuged separated from product solution after that wash it with di water. Oven at 110°C for 12h. Crush the catalyst to powder and calcine in 50 ml/min of air flow at 500°C for 1 h and then continue to activity test in next cycle.

CHAPTER IV

RESULTS AND DISSCUSSION

The main topic of research involves the use of Sn to modify Pt/TiO_2 catalyst in the furfural hydrogenation. The oxide supports were commercial P25 TiO_2 and prepared by FSP. The Pt and Sn were loaded by wet impregnation. The results and discussion in this chapter were divided into two sections. The first section, the effect of Sn addition in the Pt catalyst supported on commercial P25 TiO_2 prepared by wet impregnation was studied. The role of Sn by changing the preparation methods of the catalyst was studied in the second section. This included switching impregnation sequences, calcination temperature change, and FSP (Flame spray pyrolysis). The characterization consisted of phase analysis analyzed by X-ray diffraction (XRD), the elements and chemical composition on the surface of materials analyzed by X-ray photoelectron spectra (XPS), BET surface area determined by nitrogen physisorption, temperature reducibility evaluated by temperature programmed reduction (TPR) and active sites of the catalyst determined by H_2 chemisorption. The activity, selectivity and stability of catalyst were evaluated by furfural hydrogenation.

4.1 Effect of tin loading in Pt/TiO_2 catalyst

In this part, various amounts of Sn were added in Pt/TiO_2 support prepared by wet impregnation.

4.1.1. The structure analysis by X-ray Diffraction (XRD)

The XRD patterns of the Pt/TiO_2 and $Pt/Sn/TiO_2$ catalysts were shown in **Figure 13**. The main peaks of TiO_2 anatase phase were indicated at $2\theta=25°$ 25° (major), 37°, 48°, 55°, 56°, 62°, 71°, and 75° and rutile phase at $2\theta = 28°$ (major), 36°, 42°, and 57° were observed [37-39]. The characteristic of Pt and Sn in metal or oxide could not be detected due probably to the low amount of metal (Pt and Sn) loading.
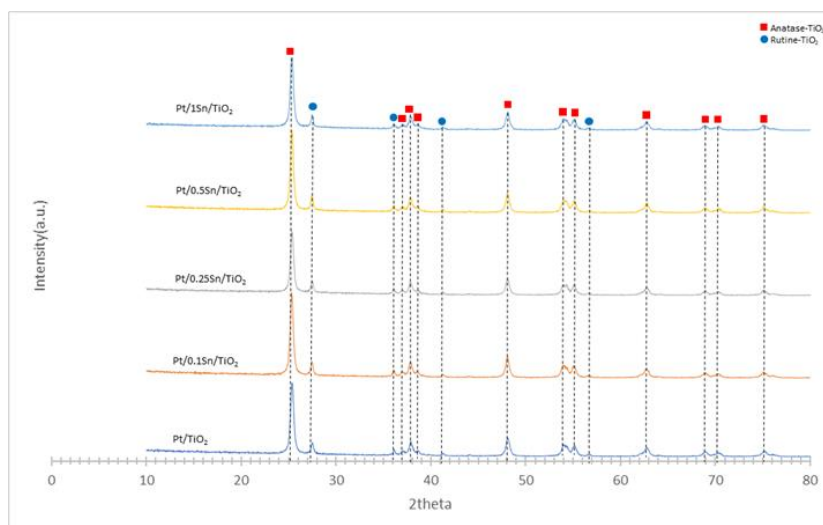
Figure 13 The XRD pattern of the Pt/Sn/TiO$_2$ catalyst with various Sn loadings.

The crystalline size of Pt/Sn/TiO$_2$ catalyst with various Sn loadings are shown in **Table 6**. It was demonstrated that addition of Sn showed the slight change of crystal size and phase composition.

Table 6 The crystalline size of the Pt/Sn/TiO$_2$ catalyst with various Sn loadings.

Catalyst	Crystalizes (nm)		Phase composition (%)	
	Anatase	Rutine	Anatase	Rutine
Pt/TiO$_2$	31.3	47.2	86.8	13.2
Pt/0.1Sn/TiO$_2$	25.1	37.8	89.8	10.2
Pt/0.25Sn/TiO$_2$	26.9	30.4	89.7	10.3
Pt/0.5Sn/TiO$_2$	34.2	37.8	87	13
Pt/1Sn/TiO$_2$	34.2	31.5	84.8	15.2

4.1.2 X-ray photoelectron spectroscopy (XPS)

In this work, the Sn3d (Sn^{2+}, Sn^{4+}, Sn) was focused at 485.5-487.1 eV. The different chemical states of Sn peaks were obtained at 485.5, 486.3 and 487.1 eV, while other two peaks at 486.3 and 487.1 eV corresponded to oxidation states of Sn [40]. As for Pt4f, approximately 72.4 eV were found. The Pt(4f) region showed peaks because multiple oxidation states at 71.0-77.5 eV could be assigned to Pt metal, Pt^{2+} and Pt^{4+} [41, 42]. From the results of the analysis, it was found that the amount of tin added was too small, therefore the deconvolution of XPS spectra could not be analyzed.

4.1.3 The specific surface area by nitrogen physisorption

The BET surface area and total pore volume are shown in **Table 7**. It was demonstrated that the BET surface area was decreased by adding the Sn while the pore volume was rather similar.

Table 7 The results from N_2 physisorption of the Pt/Sn/TiO$_2$ catalyst with various Sn loadings.

Catalyst	BET surface (m^2/g cat.)	Pore volume (cm^3/g cat.)
Pt/TiO$_2$	53.7	12.3
Pt/0.1Sn/TiO$_2$	47.2	10.8
Pt/0.25Sn/TiO$_2$	48.1	11.0
Pt/0.5Sn/TiO$_2$	48.7	11.2
Pt/1Sn/TiO$_2$	47.7	10.5

4.1.4. The reduction characteristics by temperature programmed reduction (TPR)

The TPR profiles of all samples are shown in **Figure 14**. The peak at around 80-190 °C was associated to the reduction of PtO_x crystallites to metallic Pt. Reduction of the surface capping oxygen of TiO_2 has been discovered around 360-500°C. In adding Sn, the reduction of SnO_2 appeared in the approximate temperature range of 410-473°C. But as the amount of Sn increases, aggregation of Pt and Sn to PtSn alloy may be occurred. It was reduction around 750°C. It was found in Sn 0.5% or higher adding [15]. The Sn addition resulted in a lower reduction in PtO_x temperature.
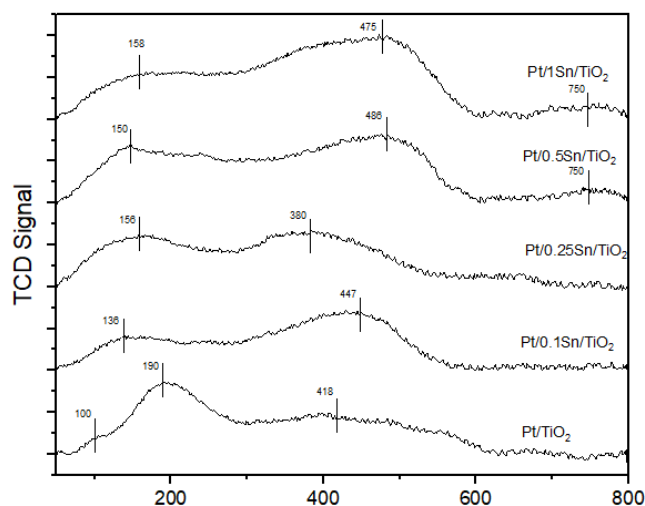
Figure 14 TPR profiles of the $Pt/Sn/TiO_2$ catalyst with various Sn loadings.

4.1.5. The metal active sites determined by H_2 chemisorption

H_2 chemisorption was used to determine amounts of active sites Pt metal on the catalysts at 100 °C. Addition of Sn affected the Pt active sites slightly except in 0.5%Sn, the active site volume was observed to be increasing sites by H_2 chemisorption shown in **Figure 15**. Addition of Sn modified Pt/TiO_2 catalysts to achieve the optimum state for furfural hydrogenation reaction, but the addition of Sn beyond a certain amount decreased the activity due to blockage of active sites [43].
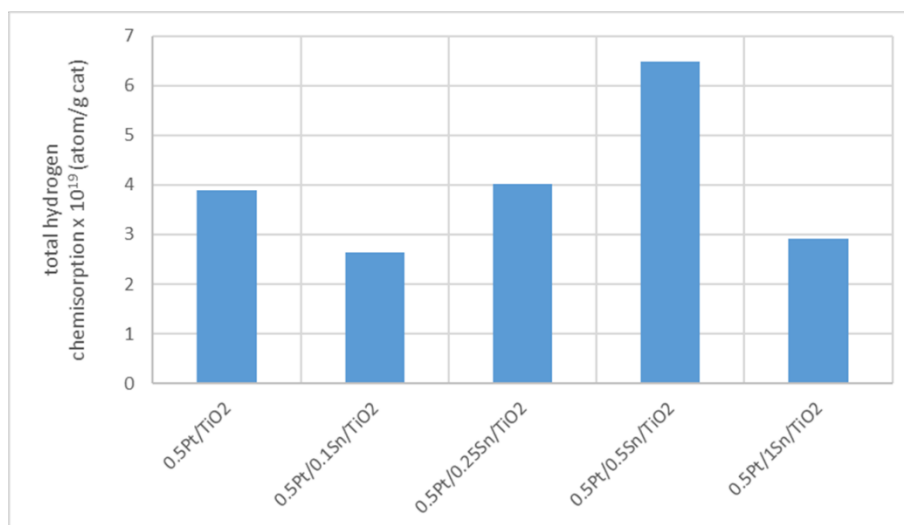
Figure 15 The amount of absorbed hydrogen of the Pt/Sn/TiO$_2$ catalyst with various Sn loadings.

4.1.6 Hydrogenation of furfural to furfuryl alcohol reaction

The furfural conversion and selectivity to FA over Pt/TiO$_2$ catalyst were 60% and 19%, respectively. For Pt/TiO$_2$ development with Sn addition, furfural conversion and selectivity to FA increased. It was evident that Sn addition over 0.1 %wt showed high conversion and selectivity to 100% and 94% shown in **Figure 16**. Improvement in furfural conversion upon Sn addition was correlated to the amount of Pt active sites. With more Pt active sites and SnO$_2$, these ionic Sn species promoting the attack of hydrogen to the carbonyl group of the furfural in which oxygen atom in the C=O group of furfurals could be coordinated via a lone pair of electrons.
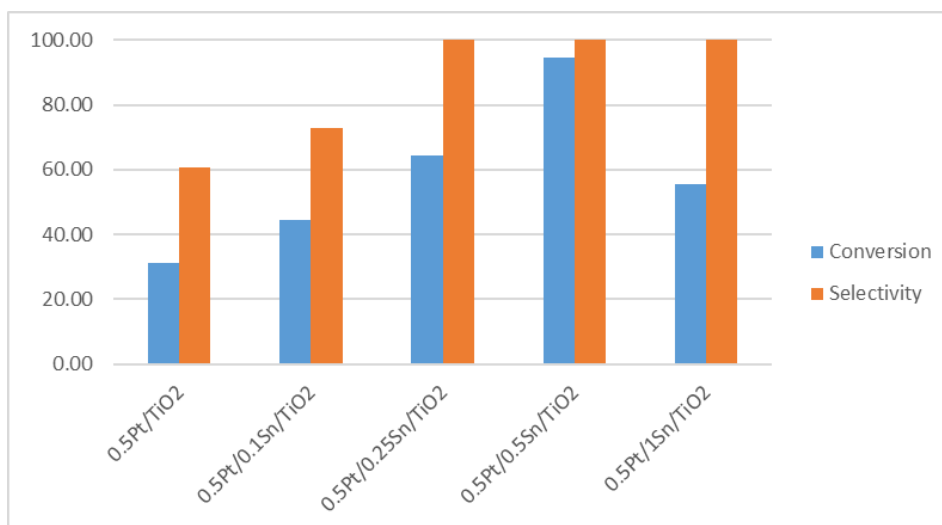
Figure 16 The hydrogenation of furfural with various catalysts at 70 °C for 2 h.

4.1.7 Reusability of catalyst for hydrogenation of furfural to furfuryl alcohol

The addition of Sn to the Pt/TiO_2 catalyst showed a change in furfuryl alcohol with a slight decrease in each hydrogenation cycle compared to no Sn adding shown in **Figure 17**. It was possible that the activity change was the result of the presence of organic matter accumulated on the catalyst [44]. Calcination of the catalyst after the reaction may help to reduce the accumulation of organic matter before reuse. But at the same time, the use of high temperature to re-calcine in the next cycle may result in the loss of active sites [32, 45, 46]. as a result of the agglomeration of platinum at repeated high-temperature calcination cycles.
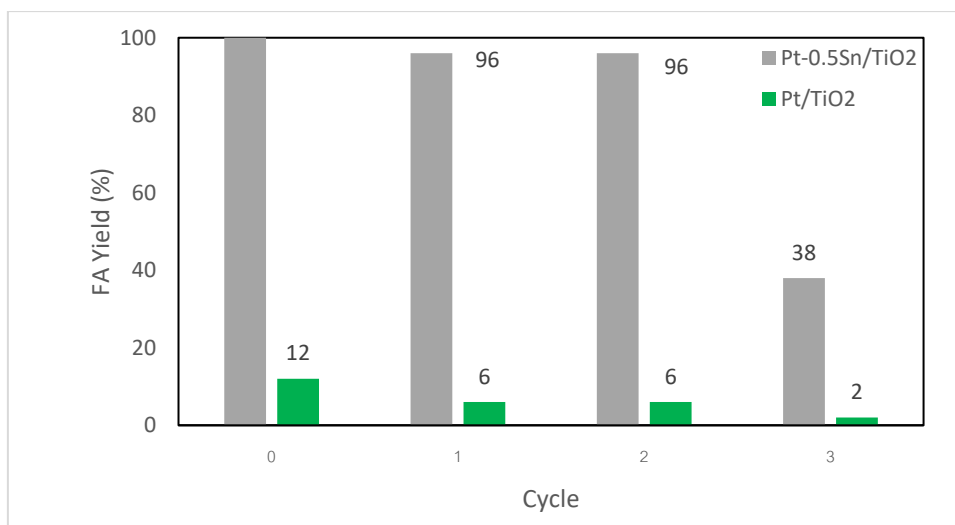
Figure 17 Reusability of catalyst for three cycles.

4.2 Role of Sn by changing the preparation methods

The promising catalyst in the first part was the Pt/0.5Sn/TiO$_2$. Three methods were sequence impregnation, calcination temperature change and FSP (Flame spray pyrolysis).

4.2.1 Sequence impregnation

The catalyst prepared by impregnation of Pt after Sn (Pt/0.5Sn/TiO$_2$), impregnation of Sn after Pt (0.5Sn/Pt/TiO$_2$) and simultaneous impregnation of Pt and Sn (Pt-0.5Sn/TiO$_2$) was compared.

4.2.1.1 The specific surface area by nitrogen physisorption.

The BET surface area and total pore volume are shown in **Table 8**. It was demonstrated that the BET surface area and pore volume were rather similar.

Table 8 The results from N_2 physisorption of the Pt/Sn/TiO$_2$ catalyst with sequence impregnation

Catalyst	BET surface (m^2/g cat.)	Pore volume (cm^3/g cat.)
Pt/0.5Sn/TiO$_2$	48.7	11.2
Pt-0.5Sn/TiO$_2$	45.3	8.3
0.5Sn/Pt/TiO$_2$	44.8	9.2

4.2.1.2 The reduction characteristics by temperature programmed reduction (TPR)

The TPR profiles of all samples are shown in **Figure 18.** It was found that the sequence of the Sn addition had an effect on the reduction temperature. The impregnation of Sn after Pt and simultaneous impregnation of Pt and Sn resulted in the reduction peak of PtO$_x$ shifted to high temperature. It was difficult to reduce. At the same time, the amount of SnO$_2$ reduced in the range of 400-500°C was increased.
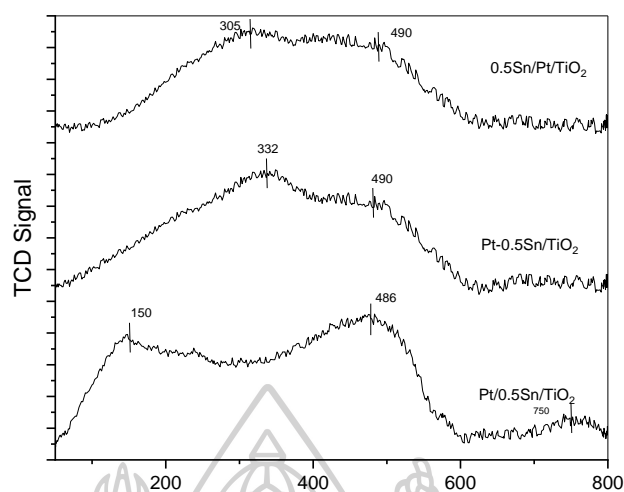
Figure 18 TPR profiles of the Pt/Sn/TiO$_2$ catalyst with various sequence impregnation.

4.2.1.3 The metal active H$_2$ chemisorption use to determine

H$_2$ chemisorption use to determine amounts of active sites platinum metal on the catalysts at 100 °C. The sequence of impregnation affected Pt sites. The active sites volume by H$_2$ chemisorption was decreased as shown in **Figure 19**. This was due to the excessive dispersion of Sn resulting in poor dispersion of Pt.
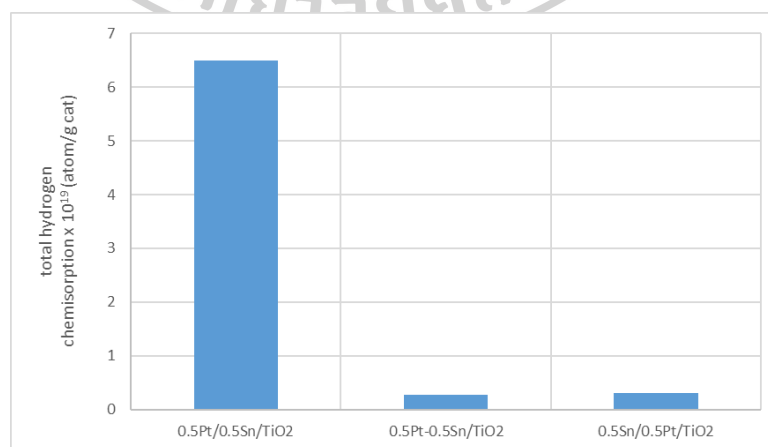
Figure 19 The amount of absorbed hydrogen of the Pt/Sn/TiO$_2$ catalyst with sequence impregnation.

4.2.1.4 The metal active sites determined by H2 chemisorption

The furfural conversion and selectivity to FA over Pt/0.5Sn/TiO$_2$ catalyst prepared by three methods of sequence impregnation as shown in **Figure 20.** Compared to the measured active sites, it was found that the catalyst prepared by impregnation of Pt after Sn gave good performance. This may be due to the presence of Sn on the surface, which can significantly reduce the formation of coke and split H$_2$ to hydrogenate furfural [47].
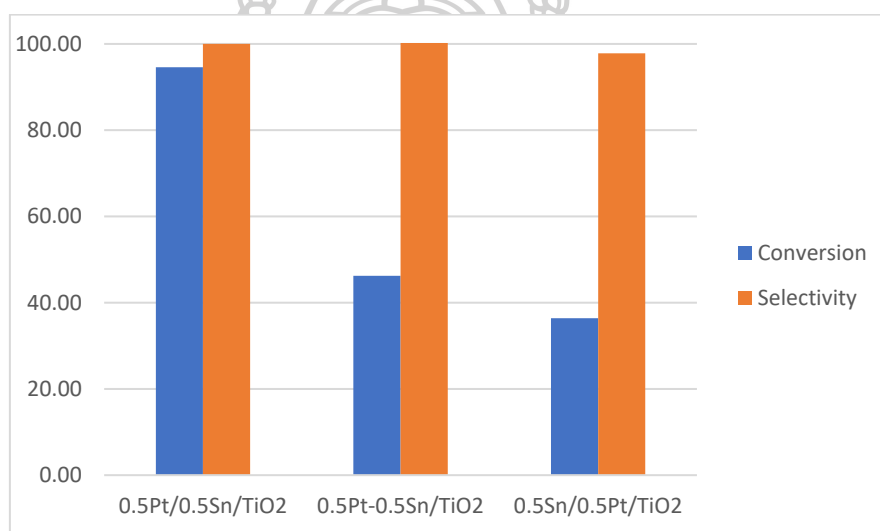
Figure 20 The hydrogenation of furfural with different sequence impregnation at 70 ℃ for 2 h.

4.2.2 Calcination temperature change

The calcination temperature was adjusted as 500℃ and 550℃ for both the step of Sn addition (Sn calcine500℃ and Sn calcine550℃) and the step of Pt addition (Pt calcine500℃ and Pt calcine550℃).

4.2.2.1 The structure analysis by X-ray Diffraction (XRD)

The XRD patterns of the Pt/Sn/TiO$_2$ catalysts at different calcination temperature as shown in **Figure 21**. The effect on the appearance of the crystal structure was the same as in the first part.
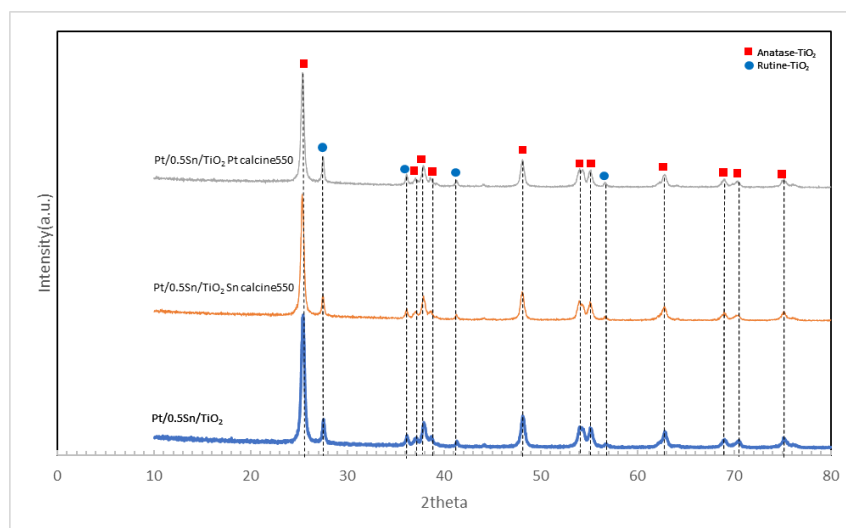
Figure 21 The XRD pattern of the Pt/Sn/TiO$_2$ catalyst at different calcination temperature.

Even with the same crystallize, an increase of temperature resulted in a TiO$_2$ anatase phase transform to rutile as shown in **Table 9**. Increasing the calcination temperature during Pt addition resulted in an increase in the crystal size of TiO$_2$ rutile phase while increasing the calcination temperature during Sn addition the crystal size remained close to the original value.

Table 9 The crystalline size of the Pt/0.5Sn/TiO$_2$ catalyst at different calcination temperature.

Catalyst	Crystalizes (nm)		Phase composition (%)	
	Anatase	Rutile	Anatase	Rutile
Pt/0.5Sn/TiO$_2$	34.2	37.8	87	13
Sn Calcine 550°C	31.3	37.7	83.6	16.4
Pt Calcine 550°C	53.7	34.3	78.9	21.1

4.2.2.2 X-ray photoelectron spectroscopy (XPS)

The result was the same as in the first section. It was found that the amount of Sn added was too small and therefore the deconvolution of XPS spectra could not be analyzed.

4.2.2.3 The specific surface area by nitrogen physisorption

The BET surface area and total pore volume are shown in **Table 10**. It was demonstrated that the BET surface area was decreased by higher calcination temperature while the pore volume was increased. The surface area can decrease because of the aggregation of particles as a result of sintering. Moreover, nanomaterials subjected to intense heat tended to have lower surface area because of the collapsing pores [48, 49].

Table 10 The results from N_2 physisorption of the Pt/Sn/TiO$_2$ catalyst with various calcination temperatures.

Catalyst	BET surface (m^2/g cat.)	Pore volume (cm^3/g cat.)
Pt/0.5Sn/TiO$_2$	48.7	11.2
Sn calcine 500°C	48.7	7.7
Sn calcine 550°C	42.4	9.7
Pt calcine 500°C	49.1	10.4
Pt calcine 550°C	45.4	11.7

4.2.2.4. The reduction characteristics by temperature programmed reduction (TPR)

The TPR profiles of all samples are shown in **Figure 22**. The reduction vertices found were similar to the study in the first section. However, increasing the calcination temperature resulted in the reduction peak of PtO$_x$ shifted to higher temperature. This may be due to the agglomeration of large particles of Pt when exposed to high temperatures.
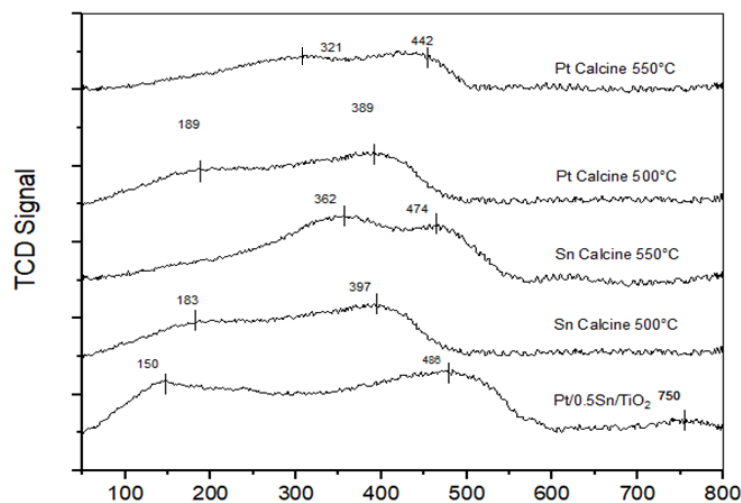
Figure 22 TPR profiles of the Pt/Sn/TiO$_2$ catalyst with various calcination temperatures.

4.2.2.5. The metal active H$_2$ chemisorption use to determine

H$_2$ chemisorption use to determine amounts of active sites platinum metal on the catalysts at 100 °C. The calcination temperature affected Pt sites. The active sites volume by H$_2$ chemisorption was decreased as shown in **Figure 23**. As a result, when the Pt particles were calcined at high temperatures, they may clump together to form larger particles. At the same time, when calcining Sn at high temperature, it may also cause tin to condense into larger particles, which affected the distribution of platinum particles.
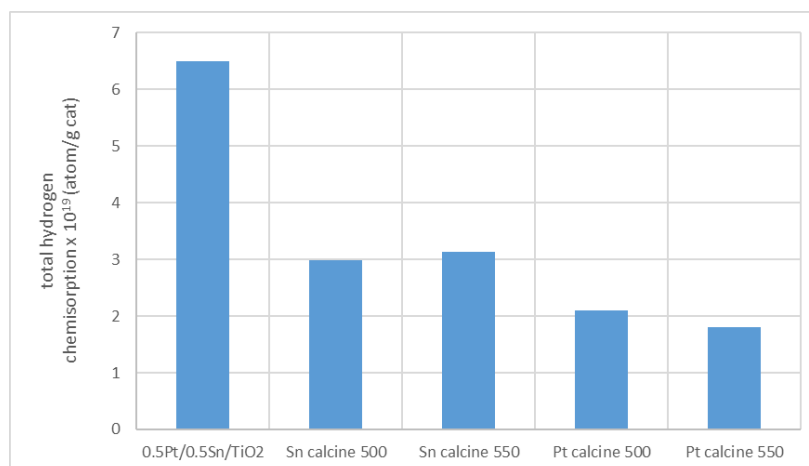
Figure 23 The amount of absorbed hydrogen of the Pt/Sn/TiO$_2$ catalyst with various calcination temperatures.

4.2.2.6 Hydrogenation of furfural to furfuryl alcohol reaction

The FOL conversion and selectivity to FA over Pt/0.5Sn/TiO$_2$ catalyst prepared by the different calcination temperature as shown in **Figure 24.** As adjusting the calcination temperature in the step of Sn addition, this resulted in reduced conversions. However, while the calcination temperature in the step of Pt addition was increased, the catalyst efficiency was greatly reduced, possibly due to the loss of active sites at high calcination temperature [50]. It may be concluded that the calcination in the step of Pt addition had a greater effect than that in the step of Sn addition.
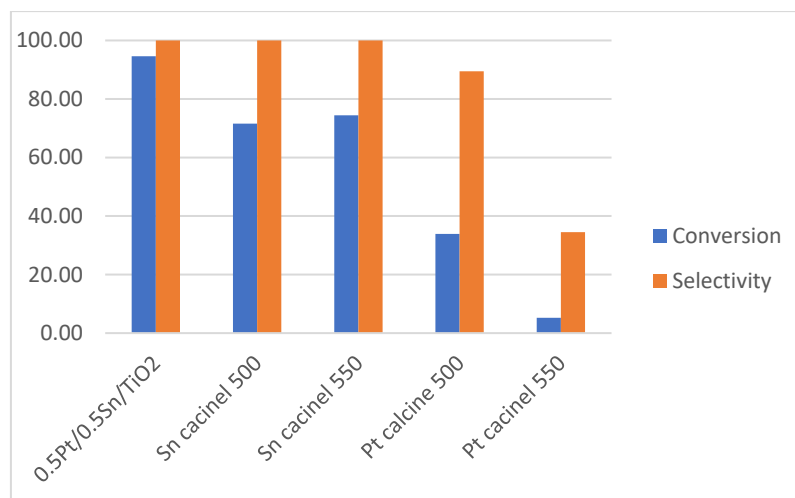
Figure 24 The hydrogenation of furfural with various calcination temperatures at 70℃ for 2 h.

4.2.2.7 Reusability of catalyst for hydrogenation of furfural to furfuryl alcohol

Three cycles of reusability were compared between the calcination temperature of 450℃ and 550℃ as shown in **Figure 25.** Due to the presence of more active sites in the Pt/0.5Sn/TiO$_2$, it showed slow deactivation compared to others.
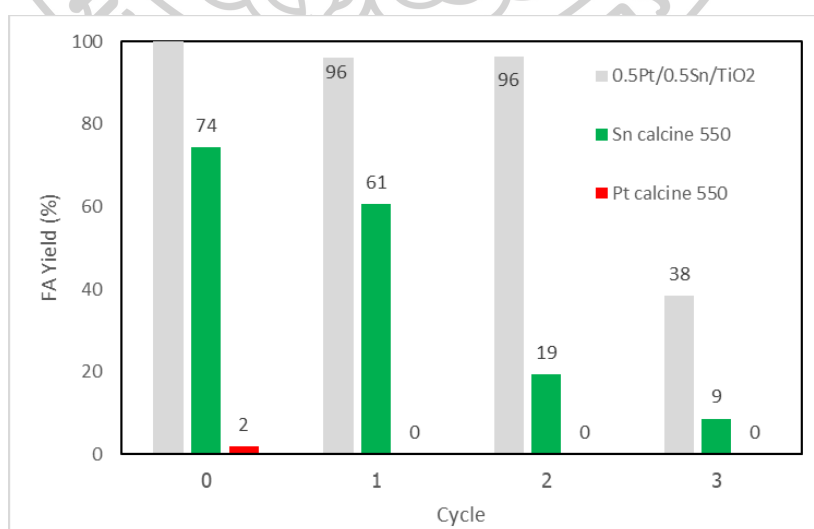
Figure 25 Reusability of catalyst for three cycles.

4.2.3 Flame spray pyrolysis method (FSP)

Two catalysts with Sn addition were prepared by flame spray pyrolysis. One was only TiO_2 prepared by FSP (Pt/0.5Sn/TiO_2 FSP) and the other was both Sn and TiO_2 prepared by FSP (Pt/0.5Sn-TiO_2 FSP).

4.2.3.1 The structure analysis by X-ray Diffraction (XRD)

The XRD patterns of the Pt/Sn/TiO_2 catalysts prepared by flame spray pyrolysis method as shown in **Figure 26**. The effect on the appearance of the crystal structure was the same as in the first part.
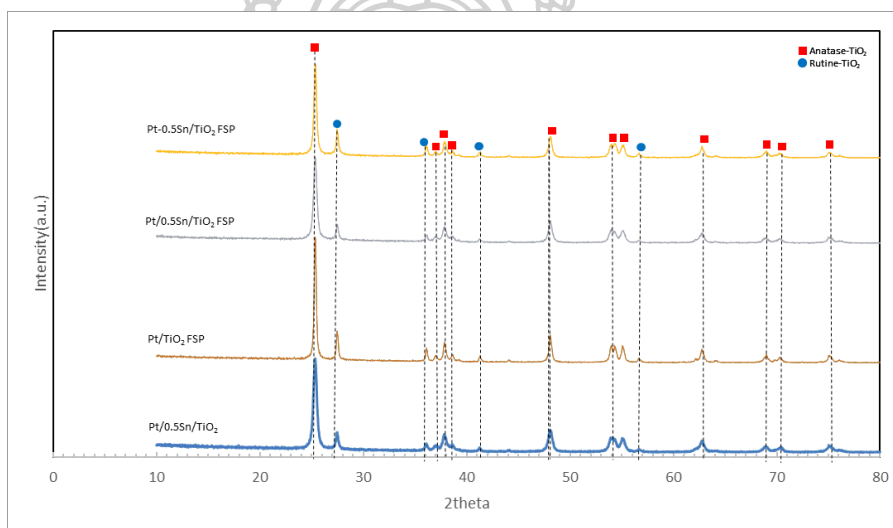
Figure 26 The XRD pattern of the Pt/Sn/TiO_2 catalyst prepared by flame spray pyrolysis method.

However, the flame spray pyrolysis method resulted in an increase of the crystal size of both anatase and rutile phases compared to the impregnation method. This may be due to an increase in temperature in the flame preparation [51]. Although there was a change in the crystal size, the ratio was similar to that of the impregnation method shown in **Table 11**.

Table 11 The crystalline size of the catalyst prepared by flame spray pyrolysis.

Catalyst	Crystalizes (nm)		Phase composition (%)	
	Anatase	Rutile	Anatase	Rutile
Pt/0.5Sn/TiO$_2$	34.2	37.8	87	13
Pt/TiO$_2$, FSP	41	53.9	85	15
Pt/0.5Sn/TiO$_2$, FSP	41.8	47.2	86.9	13.1
Pt/0.5Sn-TiO$_2$, FSP	41.8	75.4	87.2	12.8

4.2.3.2 X-ray photoelectron spectroscopy (XPS)

The result was the same as in the first section. It was found that the amount of tin added was too small and therefore the deconvolution of XPS spectra could not be analyzed.

4.2.3.3 The specific surface area by nitrogen physisorption

The BET surface area and total pore volume are shown in **Table 12.** The catalyst prepared by the flame spray pyrolysis method had smaller surface area than that prepared with commercial P25 TiO$_2$.

Table 12 The results from N_2 physisorption of the catalyst prepared by flame spray pyrolysis method**.**

Catalyst	BET surface (m^2/g cat.)	Pore volume (cm^3/g cat.)
Pt/0.5Sn/TiO$_2$	48.77	11.20
Pt/TiO$_2$ FSP	24.83	5.73
Pt/0.5Sn-TiO$_2$ FSP	34.60	7.94
Pt/0.5Sn/TiO$_2$ FSP	39.25	11.05

4.2.3.4. The reduction characteristics by temperature programmed reduction (TPR)

For the temperature programmed reduction results in **Figure 27**, the reduction peak appeared in the same way as for the first part. However, the reduction temperature of PtO$_x$ was increased for all the catalysts prepared by the flame spray pyrolysis method. It was the result of having a strong interaction between the metal and the support.
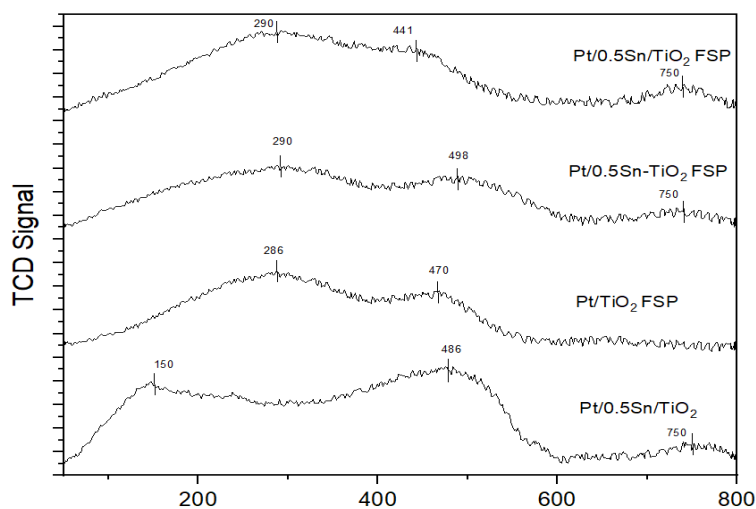
Figure 27 TPR profiles of the catalyst prepared by flame spray pyrolysis method.

4.2.3.5. The metal active H_2 chemisorption use to determine.

H_2 chemisorption use to determine amounts of active sites platinum metal on the catalysts at 100 °C. Addition of Sn for all the catalysts prepared by the flame spray pyrolysis method, the active sites by H_2 chemisorption volume were decrease shown in **Figure 28**.
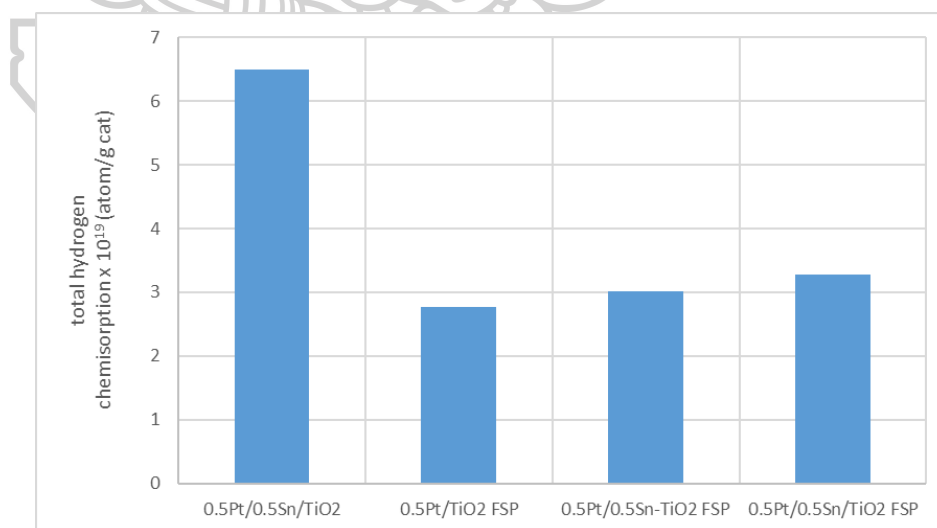
Figure 28 The amount of absorbed hydrogen of the catalyst prepared by flame spray pyrolysis method.

4.2.3.6 Hydrogenation of furfural to furfuryl alcohol reaction

Flame spray pyrolysis preparation was not as effective as impregnation preparation as shown in **Figure 29**. However, the addition of Sn also increased the catalytic yield. The simultaneous addition of Sn and TiO_2 during the FSP step showed lower yield than the FSP-TiO_2.
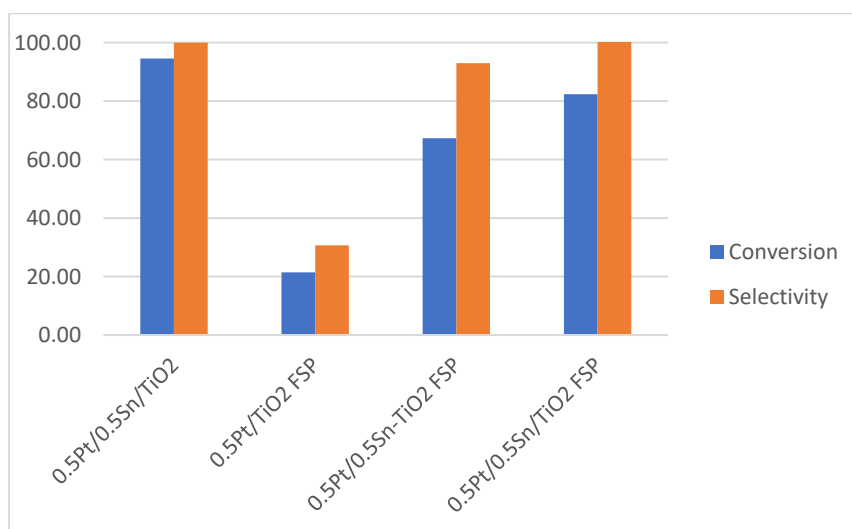
Figure 29 The hydrogenation of furfural with various catalysts 70°C for 2 h.

4.2.3.7 Reusability of catalyst for hydrogenation of furfural to furfuryl alcohol

The stability of the catalyst was shown in **Figure 30**. The flame spray pyrolysis method was unable to maintain the reusability until the first cycle. This may result in the presence of a small particle of the starting Pt sites, which were easily lost by calcination after reacting to remove organic compounds.

Figure 30 Reusability of catalyst for three cycles.

CHAPTER V

CONCLUSIONS AND RECOMMENDATION

5.1 Conclusions

In this research, roles of tin in the titania supported platinum catalyst on the selective hydrogenation of furfural to furfuryl alcohol. The experimental conclusions were summarized as follow:

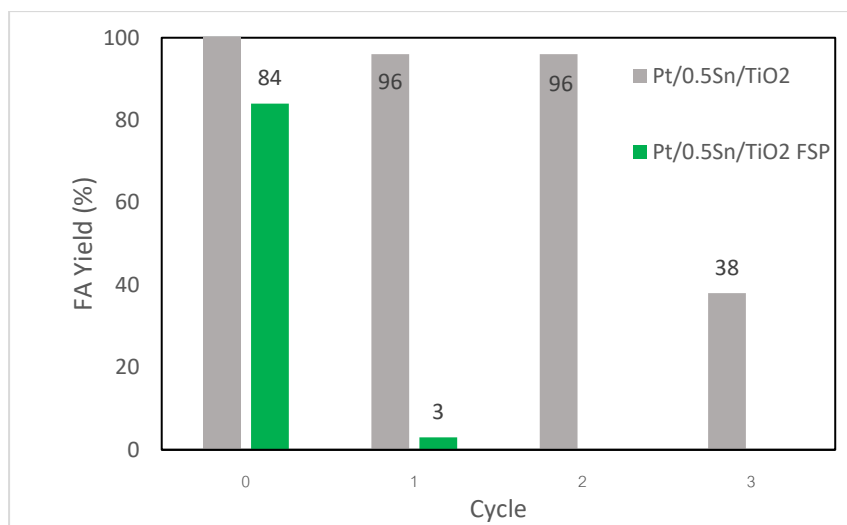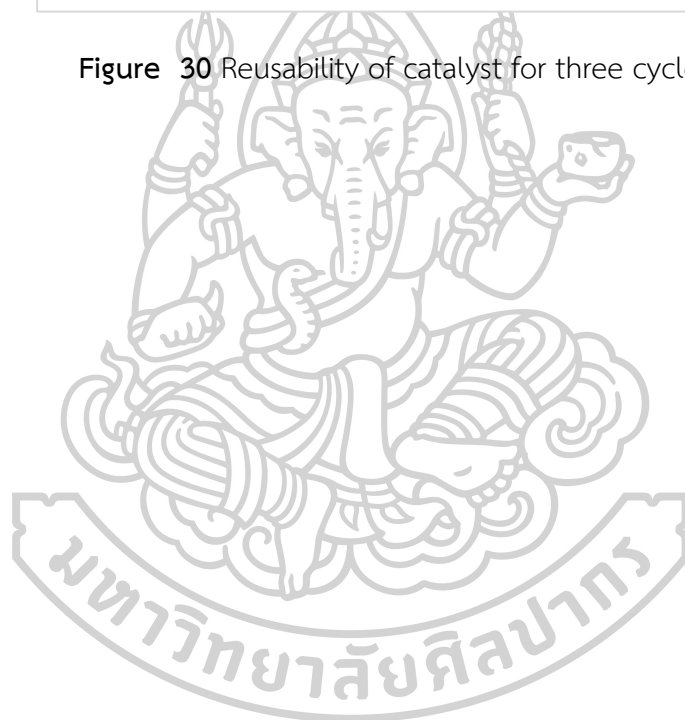1. The highest yield of FA for the Pt-based catalyst was obtained by adding the 0.5wt% Sn on commercial P25 TiO_2 prepared by wet impregnation method because the suitable Sn loading showed the highest Pt active sites.
2. For the sequence of impregnation, the impregnation of Pt after Sn showed the highest yield of FA because the Pt particles can insert during the dispersed Sn particles.
3. The high calcination temperature in the step of Pt impregnation decreased the yield of FA more than that in the step of Sn impregnation.
4. The catalyst supported on TiO_2 prepared by FSP decreased the yield of FA because the TiO_2 particles for rutile phase were large.
5. Addition of Sn in the Pt catalyst supported on both commercial P25 TiO_2 and FSP-TiO_2 showed high yield of FA.
6. Addition of Sn decelerated the catalyst deactivation, especially in the catalyst supported on commercial P25 TiO_2.
7. In this research, the Pt catalyst with Sn promoter prepared by wet impregnation method on commercial P25 TiO_2 showed the most efficiency in the furfural hydrogenation reaction.

5.2 Recommendation

The effect of formation of tin and platinum in the Pt/Sn/TiO$_2$ catalyst on the hydrogenation was still ambiguous. Due to the addition of tin and platinum in such a small quantity that the analysis value cannot be detect. Also, the cause of the deterioration in the 3rd cycle has not been confirmed. Therefore, this study was interesting.

REFERENCES

Yan, K., et al., *Production, properties and catalytic hydrogenation of furfural to fuel additives and value-added chemicals.* Renewable and Sustainable Energy Reviews, 2014. **38**: p. 663-676.

2. García-Sancho, C., et al., *Evaluation of the ZrO2/Al2O3 system as catalysts in the catalytic transfer hydrogenation of furfural to obtain furfuryl alcohol.* Applied Catalysis A: General, 2021. **609**: p. 117905.

3. O'Driscoll, Á., J.J. Leahy, and T. Curtin, *The influence of metal selection on catalyst activity for the liquid phase hydrogenation of furfural to furfuryl alcohol.* Catalysis Today, 2017. **279**: p. 194-201.

4. Mariscal, R., et al., *Furfural: a renewable and versatile platform molecule for the synthesis of chemicals and fuels.* Energy & Environmental Science, 2016. **9**(4): p. 1144-1189.

5. Wang, Y., et al., *Recent Advances in Catalytic Hydrogenation of Furfural.* Catalysts, 2019. **9**(10).

6. Fujita, S.-i., et al., *Supported liquid-phase catalysts containing ruthenium complexes for selective hydrogenation of α,β-unsaturated aldehyde: importance of interfaces between liquid film, solvent, and support for the control of product selectivity.* Journal of Catalysis, 2004. **225**(1): p. 95-104.

7. Rodiansono, R., et al., *Development of Nanoporous Ni-Sn Alloy and Application for Chemoselective Hydrogenation of Furfural to Furfuryl Alcohol.* Bulletin of Chemical Reaction Engineering & Catalysis, 2014. **9**: p. 7.

8. Tolek, W., et al., *Effects of TiO2 structure and Co addition as a second metal on Ru-based catalysts supported on TiO2 for selective hydrogenation of furfural to FA.* Scientific Reports, 2021. **11**(1): p. 9786.

9. An, K., et al., *Preparation of mesoporous oxides and their support effects on Pt nanoparticle catalysts in catalytic hydrogenation of furfural.* J Colloid Interface Sci, 2013. **392**: p. 122-128.

10. Baker, L.R., et al., *Furfuraldehyde Hydrogenation on Titanium Oxide-Supported Platinum Nanoparticles Studied by Sum Frequency Generation Vibrational Spectroscopy: Acid–Base Catalysis Explains the Molecular Origin of Strong Metal–Support Interactions.* Journal of the American Chemical Society, 2012. **134**(34): p. 14208-14216.

11. Tolek, W., et al., *Flame spray-synthesized Pt-Co/TiO2 catalysts for the selective hydrogenation of furfural to furfuryl alcohol.* Catalysis Communications, 2021. **149**: p. 106246.

12. Taylor, M.J., et al., *Atom efficient PtCu bimetallic catalysts and ultra dilute alloys for the selective hydrogenation of furfural.* Applied Catalysis B: Environmental, 2021. **284**: p. 119737.

13. Zhang, B., et al., *Influence of Sn on Stability and Selectivity of Pt–Sn@UiO-66-NH2 in Furfural Hydrogenation.* Industrial & Engineering Chemistry Research, 2020. **59**(39): p. 17495-17501.

14. Greeley, J. and M. Mavrikakis, *Alloy catalysts designed from first principles.* Nature Materials, 2004. **3**(11): p. 810-815.

15. Merlo, A.B., et al., *Bimetallic PtSn catalyst for the selective hydrogenation of furfural to furfuryl alcohol in liquid-phase.* Catalysis Communications, 2009. **10**(13): p. 1665-1669.

16. O'Driscoll, Á., et al., *Hydrogenation of Furfural with a Pt-Sn Catalyst: The Suitability to Sustainable Industrial Application.* Organic Process Research & Development, 2016. **20**: p. 1917-1929.

17. Injongkol, Y., et al., *Theoretical study on the reaction mechanism of hydrogenation of furfural to furfuryl alcohol on Lewis acidic BEA zeolites: effects of defect structure and tetravalent metals substitution.* Physical Chemistry Chemical Physics, 2017. **19**(35): p. 24042-24048.

18. Taylor, M.J., et al., *Catalytic Hydrogenation and Hydrodeoxygenation of Furfural over Pt(111): A Model System for the Rational Design and Operation of Practical Biomass Conversion Catalysts.* The Journal of Physical Chemistry C, 2017. **121**(15): p. 8490-8497.

19. Chen, X., et al., *Highly selective hydrogenation of furfural to furfuryl alcohol over Pt nanoparticles supported on g-C3N4 nanosheets catalysts in water.* Scientific Reports, 2016. **6**(1): p. 28558.

20. Taylor, M.J., et al., *Highly selective hydrogenation of furfural over supported Pt nanoparticles under mild conditions.* Applied Catalysis B: Environmental, 2016. **180**: p. 580-585.

21. Sitthisa, S., W. An, and D.E. Resasco, *Selective conversion of furfural to methylfuran over silica-supported NiFe bimetallic catalysts.* Journal of Catalysis, 2011. **284**(1): p. 90-101.

22. Rautio, A.-R., et al., *Chemoselective hydrogenation of citral by Pt and Pt-Sn catalysts supported on TiO2 nanoparticles and nanowires.* Catalysis Today, 2015. **241**: p. 170-178.

23. Jerdev, D.I., A. Olivas, and B.E. Koel, *Hydrogenation of Crotonaldehyde over Sn/Pt(111) Alloy Model Catalysts.* Journal of Catalysis, 2002. **205**(2): p. 278-288.

24. Wettstein, S.G., et al., *RuSn bimetallic catalysts for selective hydrogenation of levulinic acid to γ-valerolactone.* Applied Catalysis B: Environmental, 2012. **117-118**: p. 321-329.

25. Liu, M., et al., *Design of Highly Efficient Pt-SnO2 Hydrogenation Nanocatalysts using Pt@Sn Core–Shell Nanoparticles.* ACS Catalysis, 2017. **7**(3): p. 1583-1591.

26. Stagg, S.M., et al., *Effect of Promotion with Sn on Supported Pt Catalysts for CO2Reforming of CH4.* Journal of Catalysis, 1998. **178**(1): p. 137-145.

27. Tobaldi, D.M., et al., *Fully quantitative X-ray characterisation of Evonik Aeroxide TiO2 P25®.* Materials Letters, 2014. **122**: p. 345-347.

28. Kijeński, J., et al., *Platinum deposited on monolayer supports in selective hydrogenation of furfural to furfuryl alcohol.* Applied Catalysis A: General, 2002. **233**(1): p. 171-182.

29. Li, F., et al., *Performance of Cu/TiO2-SiO2 catalysts in hydrogenation of furfural to furfuryl alcohol.* The Canadian Journal of Chemical Engineering, 2016. **94**(7): p. 1368-1374.

30. Pisduangdaw, S., et al., *Characteristics and catalytic properties of Pt–Sn/Al2O3 nanoparticles synthesized by one-step flame spray pyrolysis in the dehydrogenation of propane.* Applied Catalysis A: General, 2009. **370**(1): p. 1-6.

31. Paulauskas, I.E.M., Deena R.; Ali, Tarek T.; El-Mossalamy, Elsayed H.; Obaid, Abdullah Y.; Basahel, Sulaiman N.; Al-Ghamdi, Ahmed A.; Sartain, Felicity K., *Photocatalytic Activity of Doped and Undoped Titanium Dioxide Nanoparticles Synthesised by Flame Spray Pyrolysis.* Johnson Matthey, 2013. **57**: p. 32-43.

32. Tang, X., et al., *MnOx–CeO2 mixed oxide catalysts for complete oxidation of formaldehyde: Effect of preparation method and calcination temperature.* Applied Catalysis B: Environmental, 2006. **62**(3): p. 265-273.

33. Gurbani, A., et al., *Comparative study of CuO–CeO2 catalysts prepared by wet impregnation and deposition–precipitation.* International Journal of Hydrogen Energy, 2009. **34**(1): p. 547-553.

34. Høj, M., et al., *Flame spray synthesis of CoMo/Al2O3 hydrotreating catalysts.* Applied Catalysis A: General, 2011. **397**(1): p. 201-208.

35. Simmance, K., et al., *Evaluation of perovskite catalysts prepared by flame spray pyrolysis for three-way catalyst activity under simulated gasoline exhaust feeds.* Catalysis Today, 2019. **320**: p. 40-50.

36. Mekasuwandumrong, O., et al., *Preparation of Nano-Pd/SiO2 by One-Step Flame Spray Pyrolysis and Its Hydrogenation Activities: Comparison to the Conventional Impregnation Method.* Industrial & Engineering Chemistry Research, 2009. **48**(6): p. 2819-2825.

37. Byun, M., et al., *Effect of surface properties of TiO2 on the performance of Pt/TiO2 catalysts for furfural hydrogenation.* RSC Advances, 2022. **12**: p. 860-868.

38. Pongthawornsakun, B., et al., *Mono- and bi-metallic Au–Pd/TiO2 catalysts synthesized by one-step flame spray pyrolysis for liquid-phase hydrogenation of 1-heptyne.* Applied Catalysis A: General, 2013. **467**: p. 132-141.

39. Zhang, J.-Y., et al., *Nanocrystalline TiO2 films studied by optical, XRD and FTIR spectroscopy.* Journal of Non-Crystalline Solids, 2002. **303**(1): p. 134-138.

40. Ramallo-López, J., et al., *XPS and XAFS Pt L 2,3 Edge Studies of Dispersed Metallic Pt and PtSn Clusters on SiO 2 Obtained by Organometallic Synthesis: Structural and Electronic Characteristics.* Journal of Physical Chemistry B - J PHYS CHEM B, 2003. **107**: p. 11441-11451.

41. Bera, P., et al., *Ionic dispersion of Pt over CeO2 by the combustion method: structural investigation by XRD, TEM, XPS, and EXAFS.* Chemistry of Materials - CHEM MATER, 2003. **15**.

42. Ramallo-López, J.M., et al., *XPS and XAFS Pt L2,3-Edge Studies of Dispersed Metallic Pt and PtSn Clusters on SiO2 Obtained by Organometallic Synthesis: Structural and Electronic Characteristics.* The Journal of Physical Chemistry B, 2003. **107**(41): p. 11441-11451.

43. Kim, H.S., et al., *Complete benzene oxidation over Pt-Pd bimetal catalyst supported on γ-alumina: influence of Pt-Pd ratio on the catalytic activity.* Applied Catalysis A: General, 2005. **280**(2): p. 125-131.

44. Alsharifi, M., et al., *Biodiesel production from canola oil using novel Li/TiO2 as a heterogeneous catalyst prepared via impregnation method.* Renewable Energy, 2017. **114**: p. 1077-1089.

45. Morone, A., M. Apte, and R.A. Pandey, *Levulinic acid production from renewable waste resources: Bottlenecks, potential remedies, advancements and applications.* Renewable and Sustainable Energy Reviews, 2015. **51**: p. 548-565.

46. Porter, J.F., Y.-G. Li, and C.K. Chan, *The effect of calcination on the microstructural characteristics and photoreactivity of Degussa P-25 TiO2.* Journal of Materials Science, 1999. **34**(7): p. 1523-1531.

47. Arbag, H., *Effect of impregnation sequence of Mg on performance of mesoporous alumina supported Ni catalyst in dry reforming of methane.* International Journal of Hydrogen Energy, 2018. **43**(13): p. 6561-6574.

48.   de Luna, M.D.G., et al., *Effect of catalyst calcination temperature in the visible light photocatalytic oxidation of gaseous formaldehyde by multi-element doped titanium dioxide.* Environ Sci Pollut Res Int, 2018. **25**(15): p. 15216-15225.

49.   Lei, X.F., et al., *Effect of calcination temperature on the structure and visible-light photocatalytic activities of (N, S and C) co-doped TiO2 nano-materials.* Applied Surface Science, 2015. **332**: p. 172-180.

50.   Sistani, A., N. Saghatoleslami, and H. Nayebzadeh, *Influence of calcination temperature on the activity of mesoporous CaO/TiO2–ZrO2 catalyst in the esterification reaction.* Journal of Nanostructure in Chemistry, 2018. **8**(3): p. 321-331.

51.   Baranwal, R., et al., *Flame Spray Pyrolysis of Precursors as a Route to Nano-mullite Powder: Powder Characterization and Sintering Behavior.* Journal of the American Ceramic Society, 2001. **84**(5): p. 951-961.
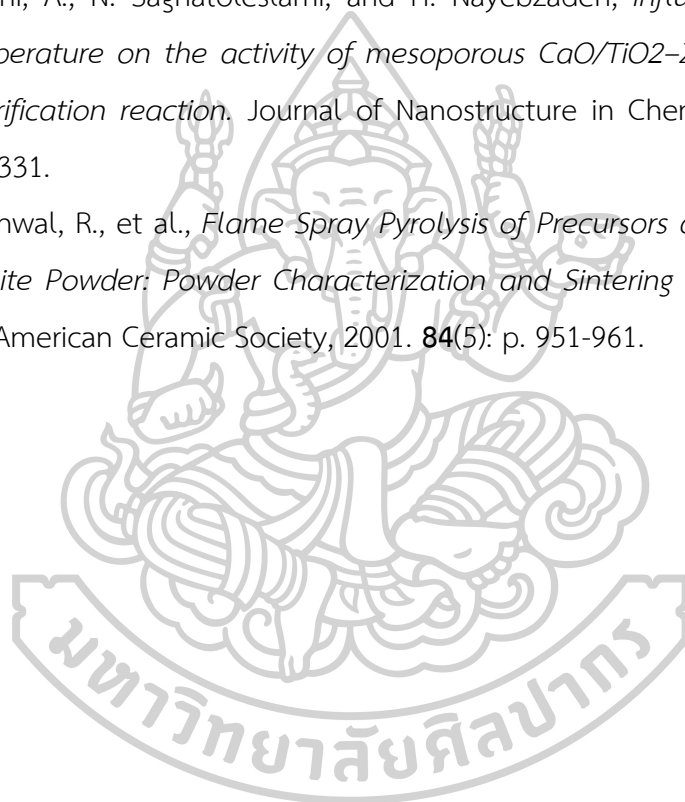
APPENDIX A

CALCULATION FOR REDUCIBILITY

For support platinum catalyst, it can be assumed that the major species of calcined Pt catalyst is PtO_2. H_2 consumption to reduce PtO_2 is calculation as follows:

Molecular weight of Pt = 195.084

Molecular weight of PtO_2 = 227.07

Calculation of the calibration of H_2 consumption using platinum oxides (PtO_2)

Let the weight of PtO_2 used = 0.1 g

= 4.4×10^{-4} mole

From equation of PtO_2 reduction;

$$PtO_2 + 2H_2 \longrightarrow Pt + 2H_2O$$

Mole of H2 consumption = 2 mole of PtO_2 consumption

= $2 \times 4.4 \times 10^{-4}$

= 8.8×10^{-4} mole

Integral area of hydrogen used to reduce Co_3O_4 0.1 g = 9.42 unit

At 100 % reducibility, the amount of hydrogen consumption is 1.661×10^{-3} mole related to the integral area of Co_3O_4 after reduction 9.42 unit.

Calculation of reducibility of supported cobalt catalyst

%Reducibility =

$$\frac{\text{Amount of } H_2 \text{ uptake to reduce 1 g of catalyst x 100}}{\text{Amount of } H_2 \text{ uptake to reduce } Co_3O_4 \text{ to } Co^0 \text{ for 1 g of catalyst}}$$

Amount of H_2 uptake to reduce Co3O4 to Co0 for 1 g of catalyst

Integral area of the calcined catalyst = X unit

The amount of H2 consumption = 1.057×10^{-6} x (X) mole

Let the weight of calcined catalyst used = W g

Concentration of Pt = 0.5 %wt

Mole of Pt = [(W x 0.5/100)/195.08] mole

Mole of PtO_2 = [(W x 0.5/100)/ (2/195.08)] mole

Reducibility (%) of supported Co catalyst = $\dfrac{[1.057 \times 10^{-6} \times (X)] \times 100}{[(W \times 0.5/100) \times (2/195.08)]}$

APPENDIX B

CALCULATION FOR TOTAL H_2 CHEMISORPTION AND DISPERSION

Calculation of the total H2 chemisorption and metal dispersion of the catalyst, a stoichiometry of H2/Co =9, is assumed. The calculation procedure is as follows:

Integral area of H_2 peak after adsorption   = A unit

Integral area of 50 μl of standard H2 peak   = B unit

Amounts of H_2 adsorbed on catalyst = B-A unit

Concentration of Pt   = 0.5 wt%

Volume of H_2 adsorbed on catalyst   = 100 × [(B-A)/B] μl

Volume of 1mole of H_2 at 100°C   = 30.61×10^{-6} μl

Mole of H2 adsorbed on catalyst   = 2x[(B-A)/B] x [50/ 30.61] mole

    = C

Total hydrogen chemisorption   = C / 0.1 mole/g cat.

The amount of adsorbed H_2 = (C / 0.1) x 6.02 x10^{23} atom/g cat.

    = D atom/g cat.

Molecular weight of cobalt   = 58.93 g/g mole

Total amount of cobalt active sites expected to exist after reduction

$$= \frac{[\%\text{reduction x (amount of Pt on catalyst/ g cat.) x } 6.02 \times 10^{23}]}{58.93}$$

$$= E$$

$$\%\text{Pt dispersion} = \frac{\text{The amount of cobalt equivalent to H2 adsorption after reduction x 100}}{\text{Total amount of cobalt active sites expected to exist after reduction}}$$

$$= [D/E] \times 10$$

APPENDIX C

CALCULATION OF THE CRYSTALLITE SIZE

Calculation of the crystallite size by Debye-Scherrer equation

The crystallite size was calculated from the half-height width of the diffraction peak of XRD pattern using the Debye-Scherrer equation.
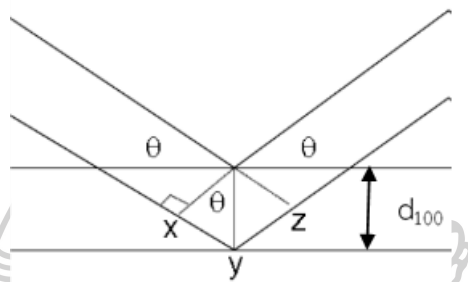
Figure 31 Derivation of Bragg's Law for X-ray

$$xy = yz = d\sin\theta$$

Thus $$xyz = 2d\sin$$

But $$xyz = n\lambda$$

Therefore $$2d\sin\theta = n\lambda$$

Bragg's Law $$d = \frac{n\lambda}{2d\sin\theta}$$

The Bragg's law was derived to D.1

From Scherrer equation:

$$\text{Crystallite size} = \frac{K\lambda}{B\cos\theta}$$

Where K   = Crystallite-shape factor = 0.9

Λ   = X-ray wavelength, 1.5418 Å for CuKα

θ   = Observed peak angle, degree

B   = X-ray diffraction broadening, radian calculated by

Warren equation

From Warren's formula:

$$B = \sqrt{B_M^2 - B_S^2}$$

Where B_M = The measured peak width in radians at half peak height.

B_S = The corresponding width of the standard material.
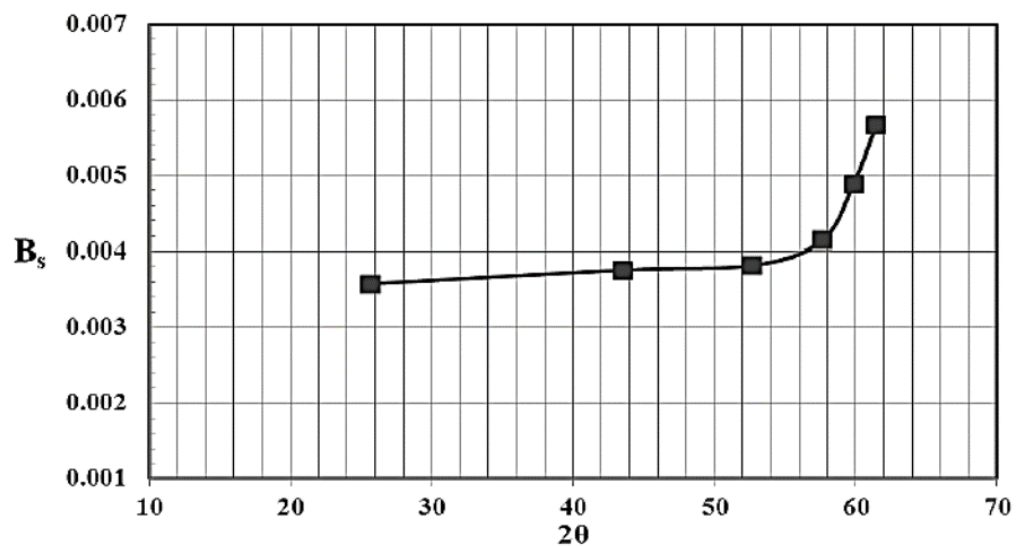
Figure 32 *The standard width of reference α-alumina sample*

59

Example: Calculation of the crystallite size of Pt/TiO$_2$
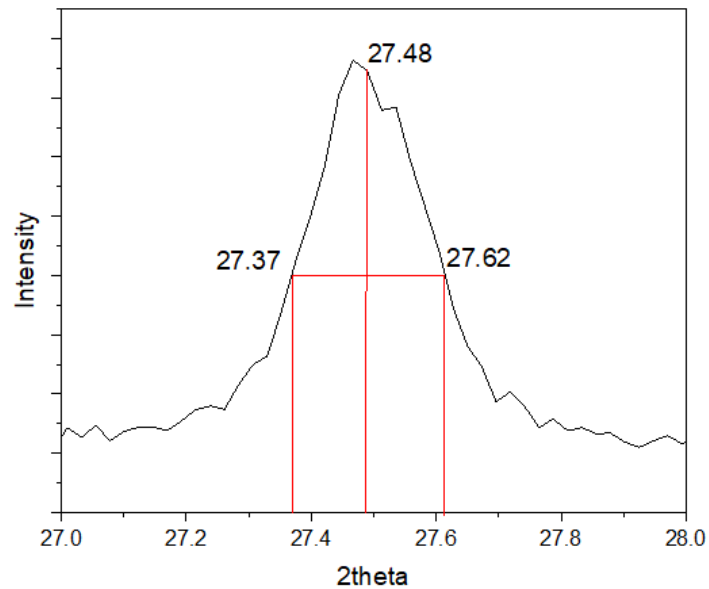
Figure 33 *The half-height width of Anatase TiO$_2$ at 27.48°*

The half-height width of titania at 27.48°　　= 0.25 (from Figure D.3)

$$= 0.25 \times (\pi/180)$$

$$= 0.0044 \text{ radian}$$

The corresponding half-height width of peak of α-alumina (from the BS value at the

2θ of 27.48° in Figure A.2) = 0.0035 radian

The peak width, 　　　　　　　　　　　B　　$= \sqrt{B_M^2 - B_S^2}$

　　　　　　　　　　　　　　　　　　B　　$= \sqrt{0.0044^2 - 0.0035^2}$

　　　　　　　　　　　　　　　　　　B　　= 0.0044

Where, 　　　　　　　　　　　　　　2θ　= 27.48°

$$\theta \qquad = 13.74°$$

$$\lambda \qquad = 1.5418\ \text{Å}$$

$$\text{The crystallite size} \qquad = \frac{0.9 \times 1.54180}{0.0044 \times \cos 13.74°}$$

$$= 289.726\ \text{Å} = 28.97\ \text{nm}$$

APPENDIX D

CALCULATON OF FURFURAL CONVERSION AND FURFURYL ALCOHOL SELECTIVITY

The furfural conversion and furfuryl alcohol selectivity were calculated by equation as follows:

$$\text{Conversion of furfural (\%)} = \frac{\text{Mole of furfural (in)} - \text{Mole of furfural (out)}}{\text{Mole of furfural (in)} - \text{Mole of furfural (out)}} \times 100$$

$$\text{Selectivity of furfuryl alcohol (\%)} = \frac{\text{Mole of furfuryl alcohol}}{\text{Mole of furfural (in)} - \text{Mole of furfural (out)}} \times 100$$

$$\text{Yield of furfuryl alcohol (\%)} = \frac{\text{FOL conversion (\%)} \times \text{FA selectivity(\%)}}{100}$$

y = 253.65x - 0.0706
R² = 0.9955
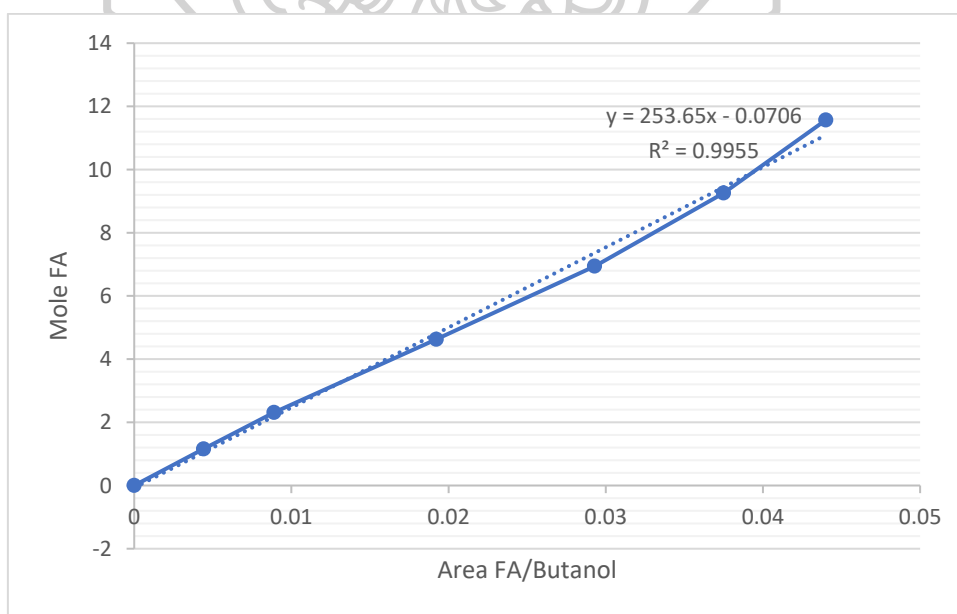
Figure 34 Calibration of furfuryl alcohol by GC-FID
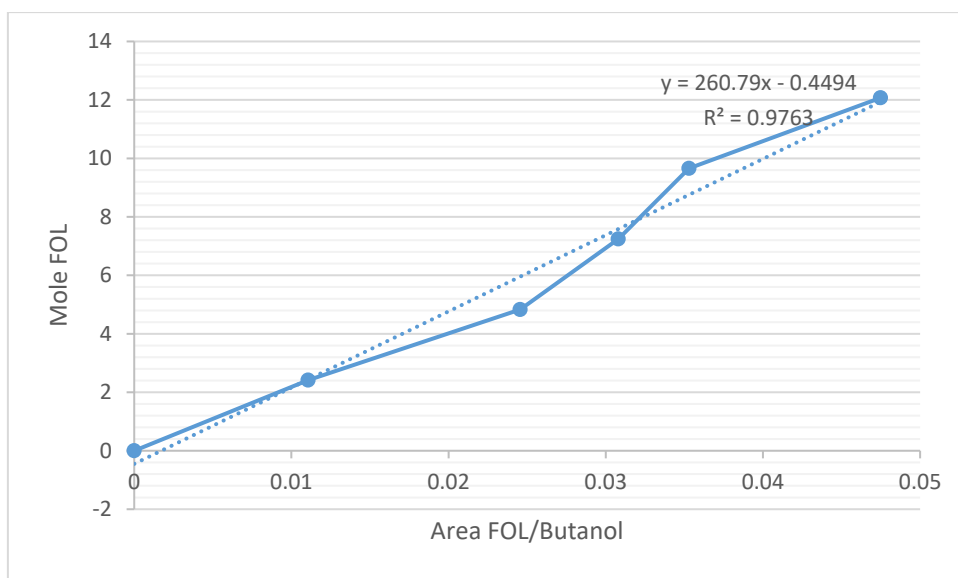
Figure 35 Calibration of furfural by GC-FID

APPENDIX E
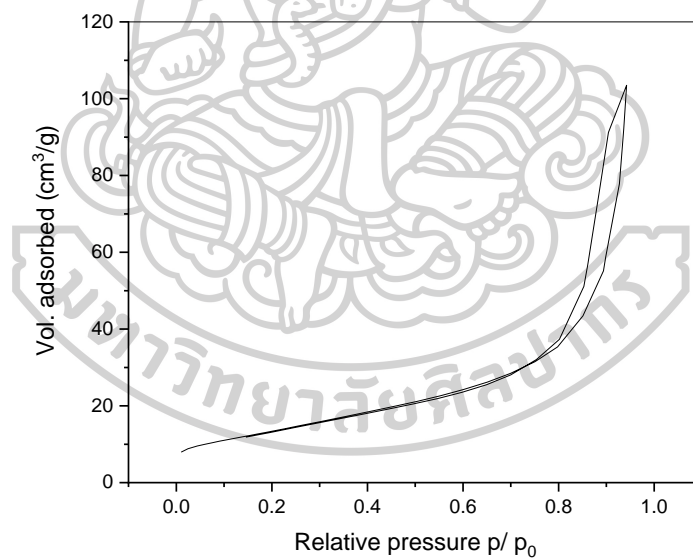
N_2 ADSORTION/DESORPTION ISOTHERMS AND PORE SIZE

DISTRIBUTION
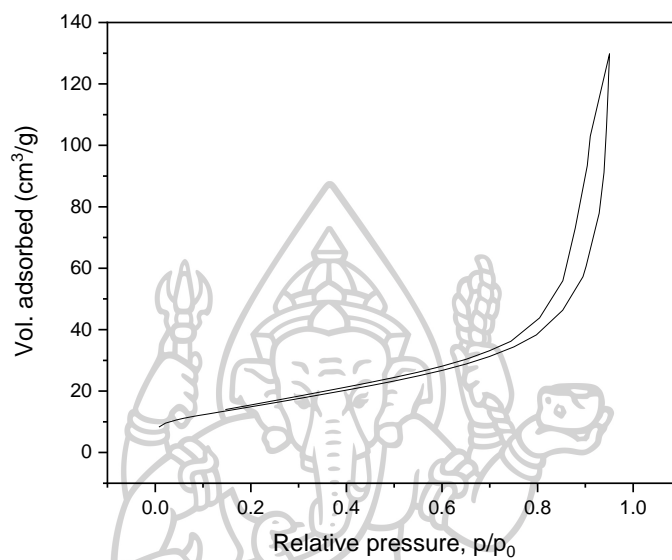
Figure 36 The N_2 adsorption/desorption isotherms for the Pt/TiO$_2$ catalyst.
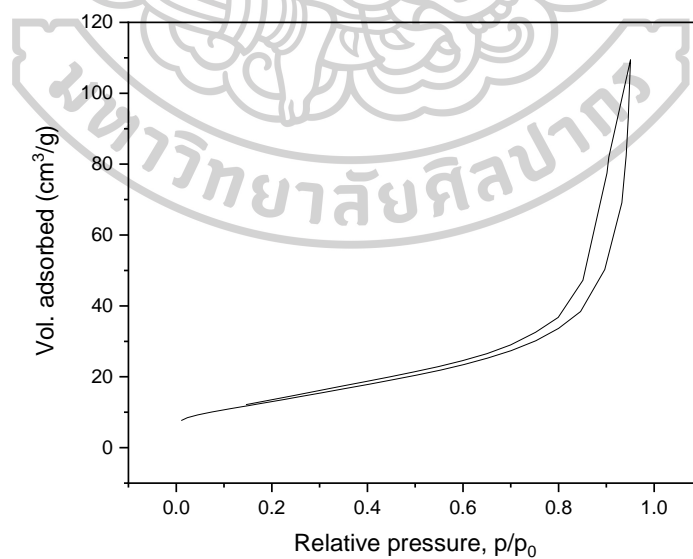
Figure 37 The N_2 adsorption/desorption isotherms for the Pt/0.1Sn/TiO$_2$ catalyst.
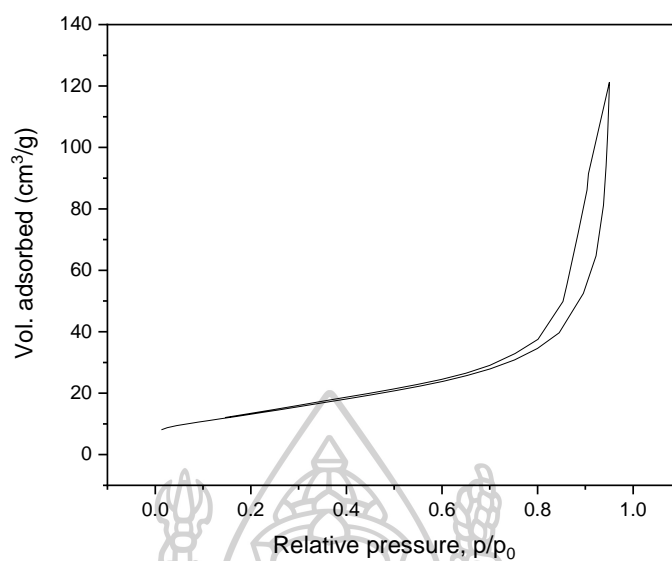
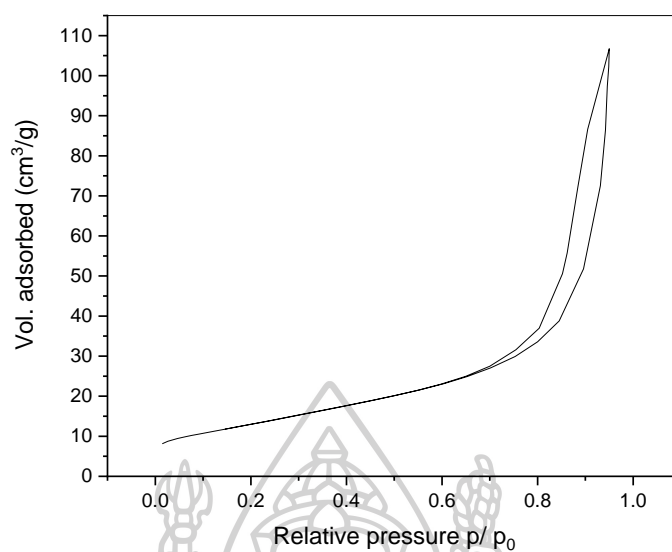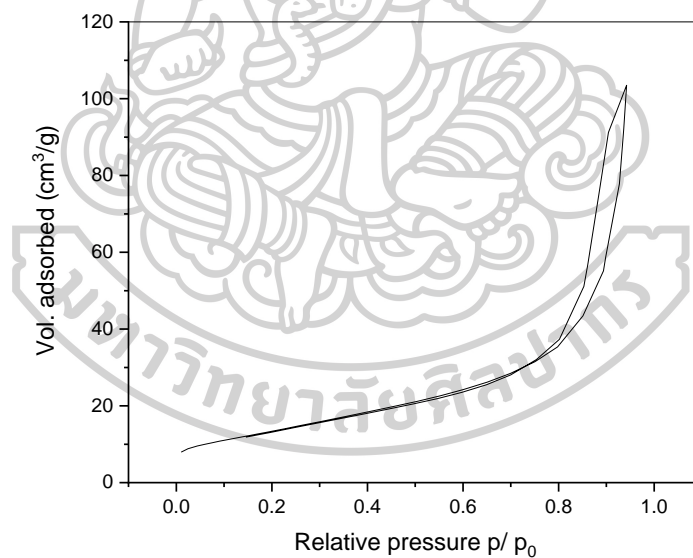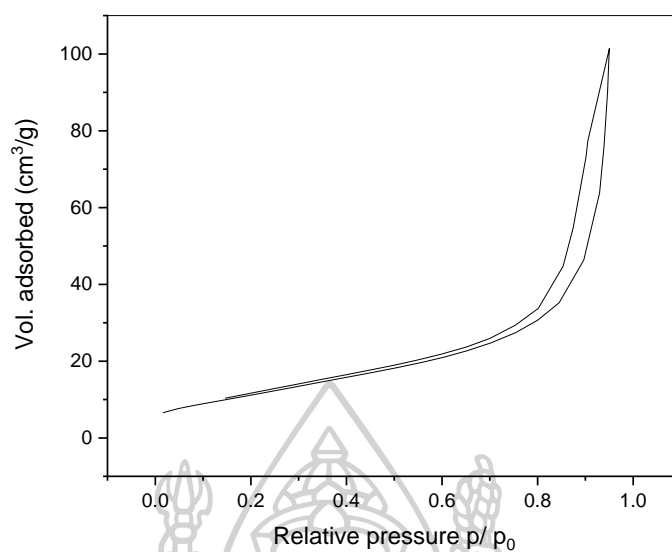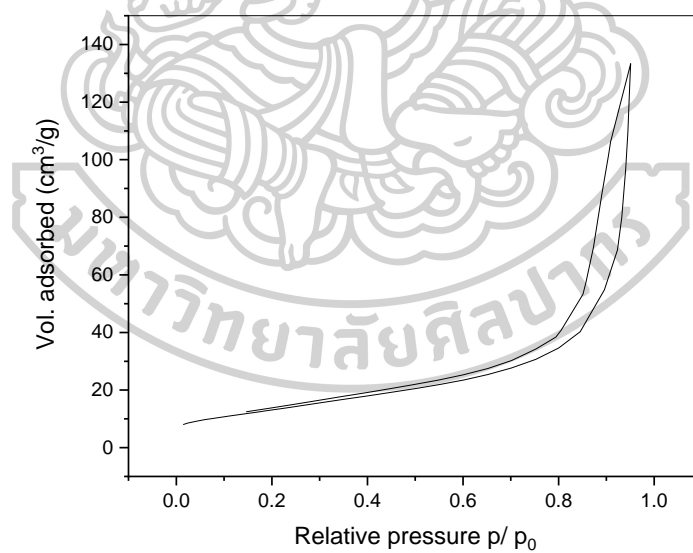**Figure 38** The N_2 adsorption/desorption isotherms for the Pt/0.25Sn/TiO$_2$ catalyst.
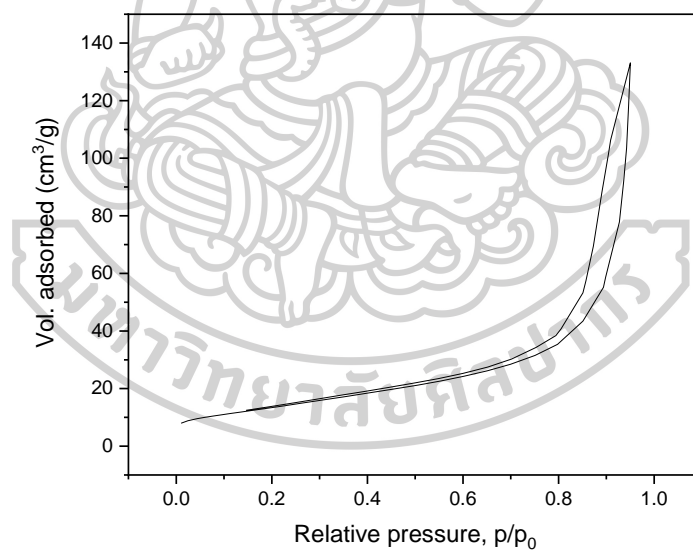
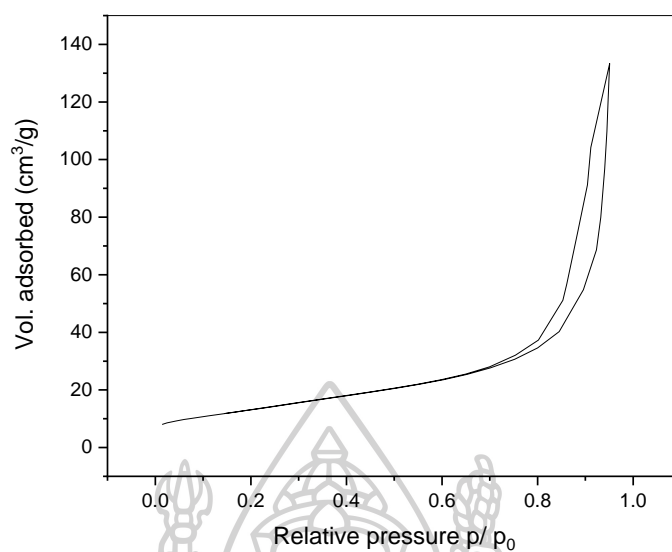**Figure 39** The N_2 adsorption/desorption isotherms for the Pt/0.5Sn/TiO$_2$ catalyst.
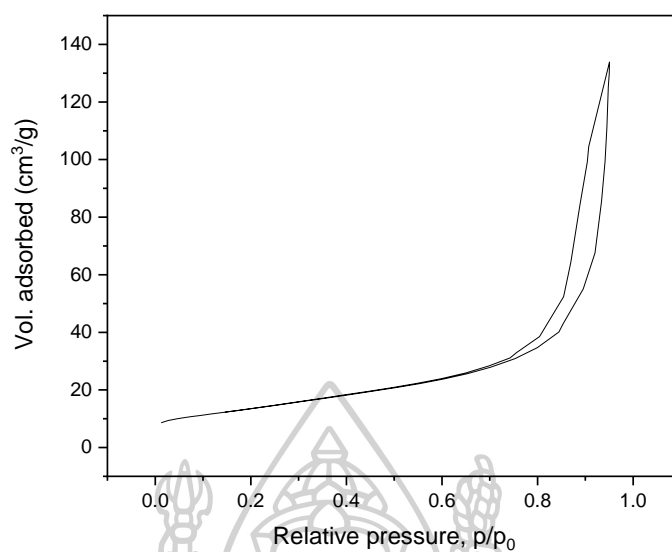
Figure 40 The N$_2$ adsorption/desorption isotherms for the Pt/1Sn/TiO$_2$ catalyst.

Figure 41 The N$_2$ adsorption/desorption isotherms for the Pt-0.5Sn/TiO$_2$ catalyst.

Figure 42 The N$_2$ adsorption/desorption isotherms for the 0.5Sn/Pt/TiO$_2$ catalyst.

Figure 43 The N$_2$ adsorption/desorption isotherms for the Pt/0.5Sn/TiO$_2$ catalyst Sn calcine 500 °C.
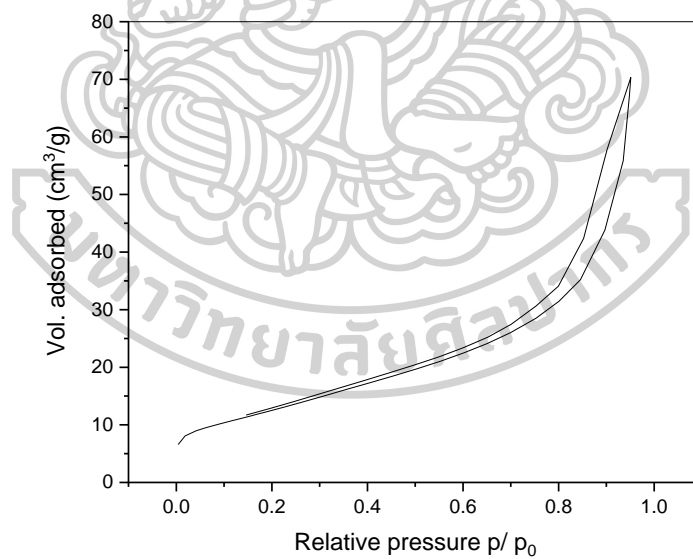
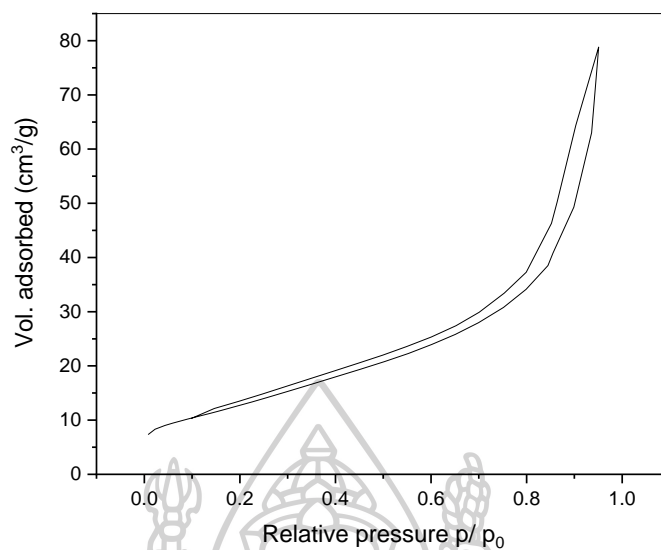**Figure 44** The N$_2$ adsorption/desorption isotherms for the Pt/0.5Sn/TiO$_2$ catalyst Sn calcine 550 °C.

Figure 45 The N$_2$ adsorption/desorption isotherms for the Pt/0.5Sn/TiO$_2$ catalyst Pt calcine 500 °C.
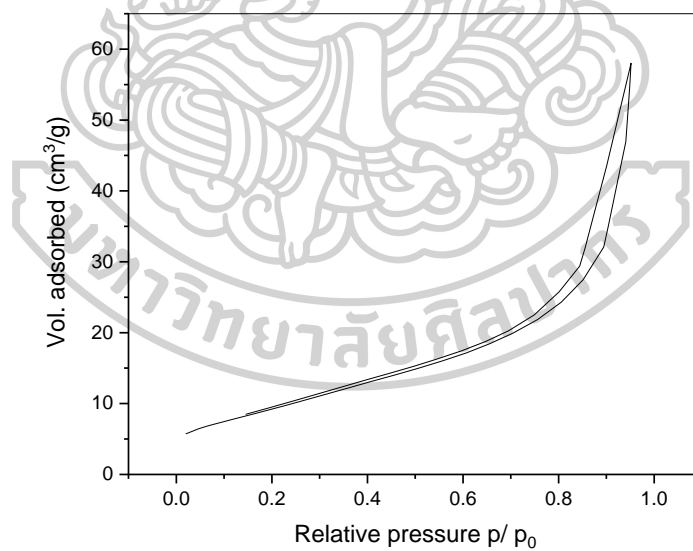
Figure 46 The N_2 adsorption/desorption isotherms for the Pt/0.5Sn/TiO$_2$ catalyst Pt calcine 550 ℃.

Figure 47 The N_2 adsorption/desorption isotherms for the Pt/TiO$_2$ FSP catalyst.

70

Figure 48 The N_2 adsorption/desorption isotherms for the Pt/0.5Sn/TiO$_2$ FSP catalyst.

Figure 49 The N_2 adsorption/desorption isotherms for the Pt/0.5Sn-TiO$_2$ FSP catalyst.
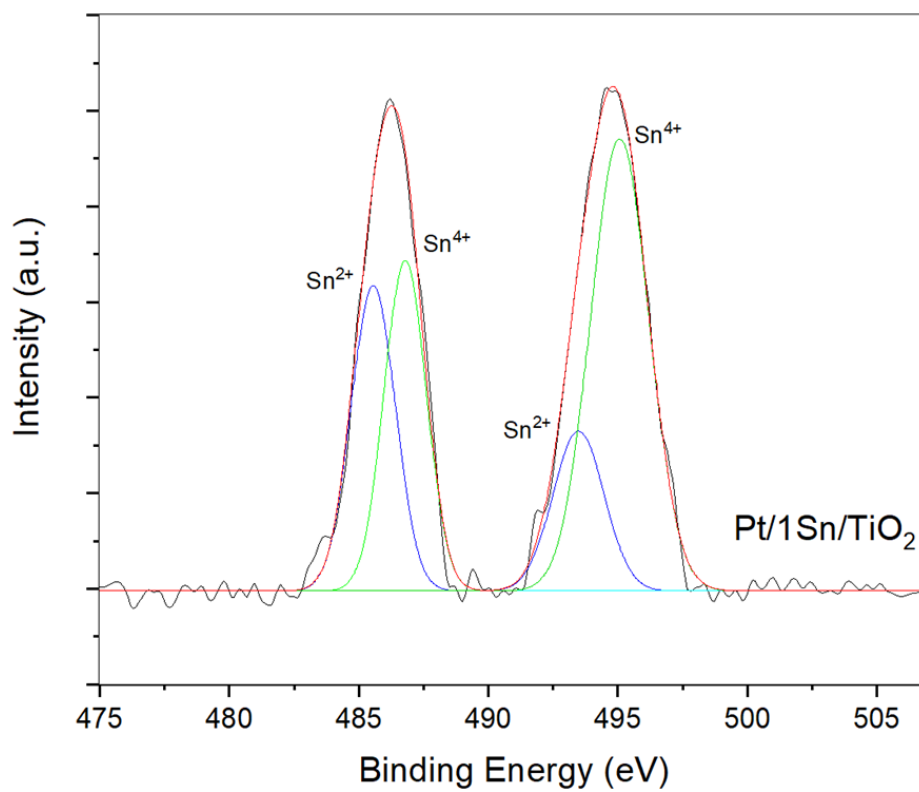
APPENDIX F

DECONVOLUTION OF GUSSIUN METHOD FOR Sn SPECIES

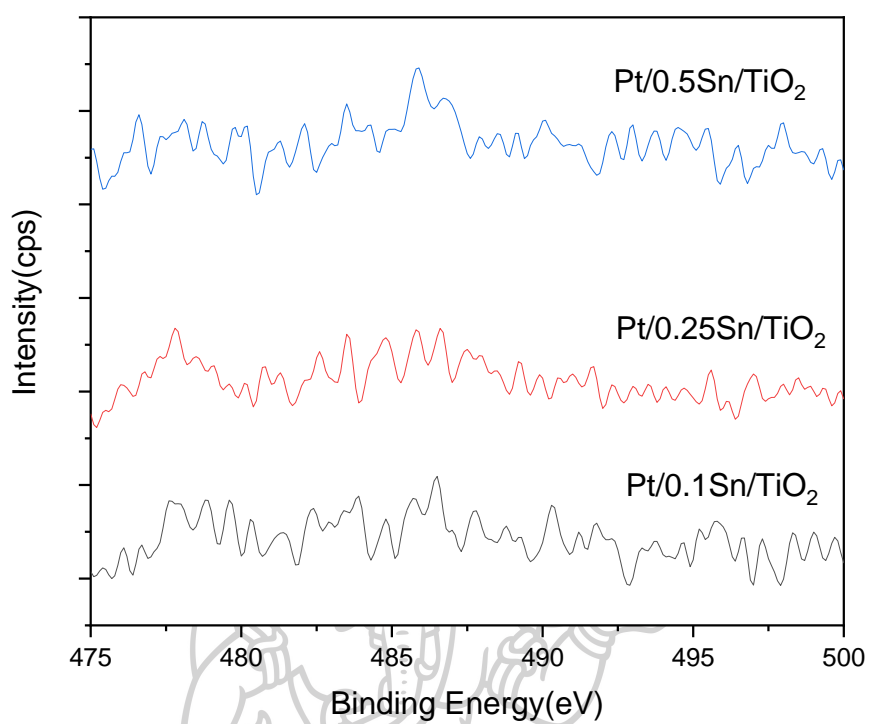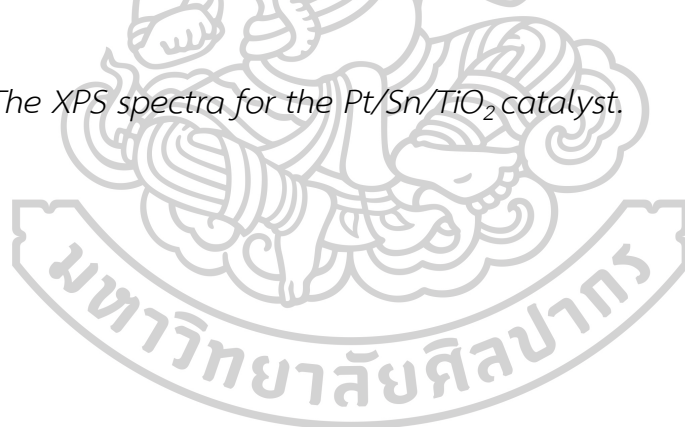*Figure 50 The deconvolution of XPS spectra for the Pt/1Sn/TiO₂ catalyst.*

Figure 51 *The XPS spectra for the Pt/Sn/TiO$_2$ catalyst.*

VITA

NAME   Nattaphat Ovatnupat

DATE OF BIRTH   13/3/1996

PLACE OF BIRTH   Bangkok Thailand

INSTITUTIONS ATTENDED   Bachelor degree of Engineering (CHEMICAL ENGINEERING)

                      Department of CHEMICAL ENGINEERING

                      Graduate School, Silpakorn University

HOME ADDRESS   139/170 Moo5 Mahasawad Sub-District Bangkruai District

                      Nonthaburi 11130